

ARO 17747.3-EG

(2)

ARVIN/CALSPAN

2D000 804026

NUMERICAL STUDIES OF FLUID SPIN-UP FROM
REST IN A PARTIALLY FILLED CYLINDER

FINAL REPORT

Calspan Report No. 6856-A-2

Gregory F. Homicz

November 1984

AD-A150 079

Prepared for:

U.S. ARMY RESEARCH OFFICE

CONTRACT NO. DAAG29-81-C-0007

Prepared by:

CALSPAN ADVANCED TECHNOLOGY CENTER

PHYSICAL SCIENCES DEPARTMENT

P.O. BOX 400

BUFFALO, NY 14225

APPROVED FOR PUBLIC RELEASE;
DISTRIBUTION UNLIMITED

DTIC
SELECT
FEB 7 1985
A

DTIC FILE COPY

ADVANCED TECHNOLOGY CENTER P.O. BOX 400 BUFFALO, NEW YORK 14225

Calspan/CALSPAN/Forms 01-278 TEL: (716) 632-7800

Reproduced From
Best Available Copy

85 01 28 087

1/14

REPORT DOCUMENTATION PAGE		READ INSTRUCTIONS BEFORE COMPLETING FORM
1. REPORT NUMBER ARO 17747.3-EG	2. GOVT ACCESSION NO. AD-A152 079	3. RECIPIENT'S CATALOG NUMBER
4. TITLE (and Subtitle) NUMERICAL STUDIES OF FLUID SPIN-UP FROM REST IN A PARTIALLY-FILLED CYLINDER		5. TYPE OF REPORT & PERIOD COVERED Final Report 3/1/81 - 9/30/84
7. AUTHOR(s) Gregory F. Homicz		6. PERFORMING ORG. REPORT NUMBER 6856-A-2
9. PERFORMING ORGANIZATION NAME AND ADDRESS Calpan Advanced Technology Center P. O. Box 400 Buffalo, NY 14225		8. CONTRACT OR GRANT NUMBER(s) DAAG29-81-C-0007
11. CONTROLLING OFFICE NAME AND ADDRESS U.S. Army Research Office Post Office Box 12211 Research Triangle Park, NC 27709		10. PROGRAM ELEMENT, PROJECT, TASK AREA & WORK UNIT NUMBERS
14. MONITORING AGENCY NAME & ADDRESS (if different from Controlling Office)		12. REPORT DATE November 1984
		13. NUMBER OF PAGES 48
		15. SECURITY CLASS. (of this report) Unclassified
		15a. DECLASSIFICATION/DOWNGRADING SCHEDULE
16. DISTRIBUTION STATEMENT (of this Report) Approved for public release; distribution unlimited.		
17. DISTRIBUTION STATEMENT (of the abstract entered in Block 20, if different from Report) NA		
18. SUPPLEMENTARY NOTES The view, opinions, and/or findings contained in this report are those of the author(s) and should not be construed as an official Department of the Army position, policy, or decision, unless so designated by other documentation.		
19. KEY WORDS (Continue on reverse side if necessary and identify by block number) Rotating Flow Liquid-Filled Shells Spin-Up		
20. ABSTRACT (Continue on reverse side if necessary and identify by block number) This is the final report describing a three year theoretical investigation of the dynamics of fluid spin-up in a partially-filled cylindrical cavity. The effort was divided into two phases. The first phase consisted of developing an extension of the earlier analyses of Nedemeyer, and of Goller and Ranov, to those cases where the liquid free surface intersects one or both endwalls. The simplifying assumptions of a columnar flow and the quasi-steady treatment of the Ekman layer pumping of the secondary flow are retained. Earlier estimates of the Ekman		

20. (Continued)

layer pumping are modified heuristically for situations where the layer(s) no longer covers the entire wall. Also, due to the very steep free surface contour in the latter stages of spin-up, it was found advantageous to develop the free surface equations in an axial, rather than radial, coordinate frame. This model and the resulting computer code are the subject of an earlier interim report and a subsequent paper submitted for journal publication. Accordingly, only a summary of this phase and its results is presented here.

No experimental or numerical data were available against which to compare the simplified model's predictions for cases where the free surface intersects one or both endwalls. Accordingly, in the second phase of the program a more refined numerical model was developed, based on the full nonlinear Navier-Stokes equations. This is a finite difference code in which the primitive variable equations are solved in conservative form. The development of the governing equations, and the semi-implicit predictor-corrector scheme used to solve them, are presented in some detail. Unfortunately, no converged solutions have been obtained as yet; the possible reasons for this are discussed.

UNCLASSIFIED

FOREWORD

This is a final report documenting the results of a three-year theoretical program "Numerical Models for Fluid Behavior During Spin-Up in Liquid-Filled Shells," sponsored by the U.S. Army Research Office under Contract No. DAAG29-81-C-0007. The program is under the technical supervision of Dr. Robert E. Singleton. Recognition is due Dr. Raymond S. Sedney and Mr. Nathan Gerber of the Launch and Flight Division, U.S. Army Ballistic Research Laboratory, who through their technical discussions with the author have had a significant impact on the course of this work. The implicit computer code which they provided, and which served as the starting point for the simplified model developed here, is also gratefully acknowledged. Finally, the author wishes to thank his colleague, Dr. William J. Rae, for his advice and encouragement.

Accession For	
NTIS GRA&I	<input checked="" type="checkbox"/>
DTIC TAB	<input type="checkbox"/>
Unannounced	<input type="checkbox"/>
Justification	
Per	
Distribution/	
Availability	
Dist	Spec

A



TABLE OF CONTENTS

<u>Section</u>		<u>Page</u>
	FOREWORD	iii
1	INTRODUCTION	1
2	SIMPLIFIED MODEL	5
	2.1 Principal Assumptions and Equations	5
	2.2 Modifications to Original Model	7
	2.3 Results	9
3	NAVIER-STOKES MODEL	14
	3.1 Governing Equations	14
	3.2 Coordinate Transformations	16
	3.3 Computational Grid	18
	3.4 Difference Equations for Velocities	20
	3.5 Difference Equation for Pressure	24
	3.6 Difference Equation for Surface Contour	30
	3.7 Overall Computational Cycle	31
	3.8 Results	33
4	CONCLUSIONS	38
	REFERENCES	40
	NOMENCLATURE	42
	APPENDIX	43
	TECHNICAL REPORTS, PUBLICATIONS	48

PREVIOUS PAGE
IS BLANK

LIST OF ILLUSTRATIONS

<u>Figure</u>	<u>Title</u>	<u>Page</u>
1	Cylindrical Geometry and Possible Fluid Configuration During Spin-Up	2
2	Numerical Results for Case 3	10
3	Angular Momentum Deficit vs. Time for Cases 3 through 5	12
4	Staggered Grid Arrangement	19
5	Pressure Boundary Condition at the Free Surface	29

1. INTRODUCTION

The goal of the theoretical program described here was to obtain a clearer understanding of the fluid dynamics of liquid-filled shells for those cases where the fluid only partially fills its cavity. Problems can arise during the flight of such projectiles when there is a strong coupling between the perturbed motion of the rapidly spinning shell casing and the attendant wave motion excited in the fluid. In addition, unlike a solid filler which always rotates with the same angular velocity as the casing, the liquid filler will rotate at a reduced angular velocity over much of the trajectory. The result is a net transfer of angular momentum from casing to fluid, which in itself can be destabilizing.¹

The model problem most often studied by investigators is the axisymmetric spin-up of fluid in a right circular cylinder of radius R (see Fig. 1). We seek to represent the evolution with time of the fluid motion, particularly the azimuthal velocity, as it asymptotically approaches solid-body rotation. Such a calculation is necessary as input for the prediction of the spin decay of liquid-filled projectiles.^{2,3} It can also serve as the base flow about which to carry out a perturbation analysis of the eigenfrequencies of the fluid.^{4,5} The latter are of critical importance to the question of the stability of the fluid-shell system.¹

A review of previous work on this problem has been given in Refs. 6 and 7 and will not be repeated here. The principal conclusion drawn from these studies is that,

1. Engineering Design Handbook. Liquid-Filled Projectile Design, AMC Pamphlet No. 706-165, U.S. Army Materiel Command, Washington, D.C., April 1969.
2. Kitchens, C.W., Jr., Gerber, N. and Sedney, R., "Spin decay of Liquid Filled Projectiles," J. of Spacecraft, Vol. 15, No. 6, 348-354, December 1978.
3. Kitchens, C.W., Jr. and Gerber, N., Prediction of Spin Decay of Liquid Filled Projectiles, BRL Report 1996, Aberdeen Proving Ground, Md., July 1977.
4. Kitchens, C.W., Jr., Gerber, N., and Sedney, R., Oscillations of a Liquid in a Rotating Cylinder: Part I. Solid-Body Rotation, ARBRL-TR-02081, Aberdeen Proving Ground, Md., June 1978.
5. Sedney, R. and Gerber, N., Oscillations of a Liquid in a Rotating Cylinder: Part II. Spin-Up, ARBRL-TR-02489, Aberdeen Proving Ground, Md., May 1983.
6. Homicz, G.F., Numerical Model for Fluid Spin-Up in a Partially-Filled Cylinder, Calspan Report No. 6856-A-1, May 1982, prepared for U.S. Army Research Office as interim report on Contract DAAG29-81-C-0007.
7. Homicz, G. F. and Gerber, N., "Numerical Model for Fluid Spin-Up from Rest in a Partially-Filled Cylinder," submitted to ASME Transactions, J. of Fluids Engineering.

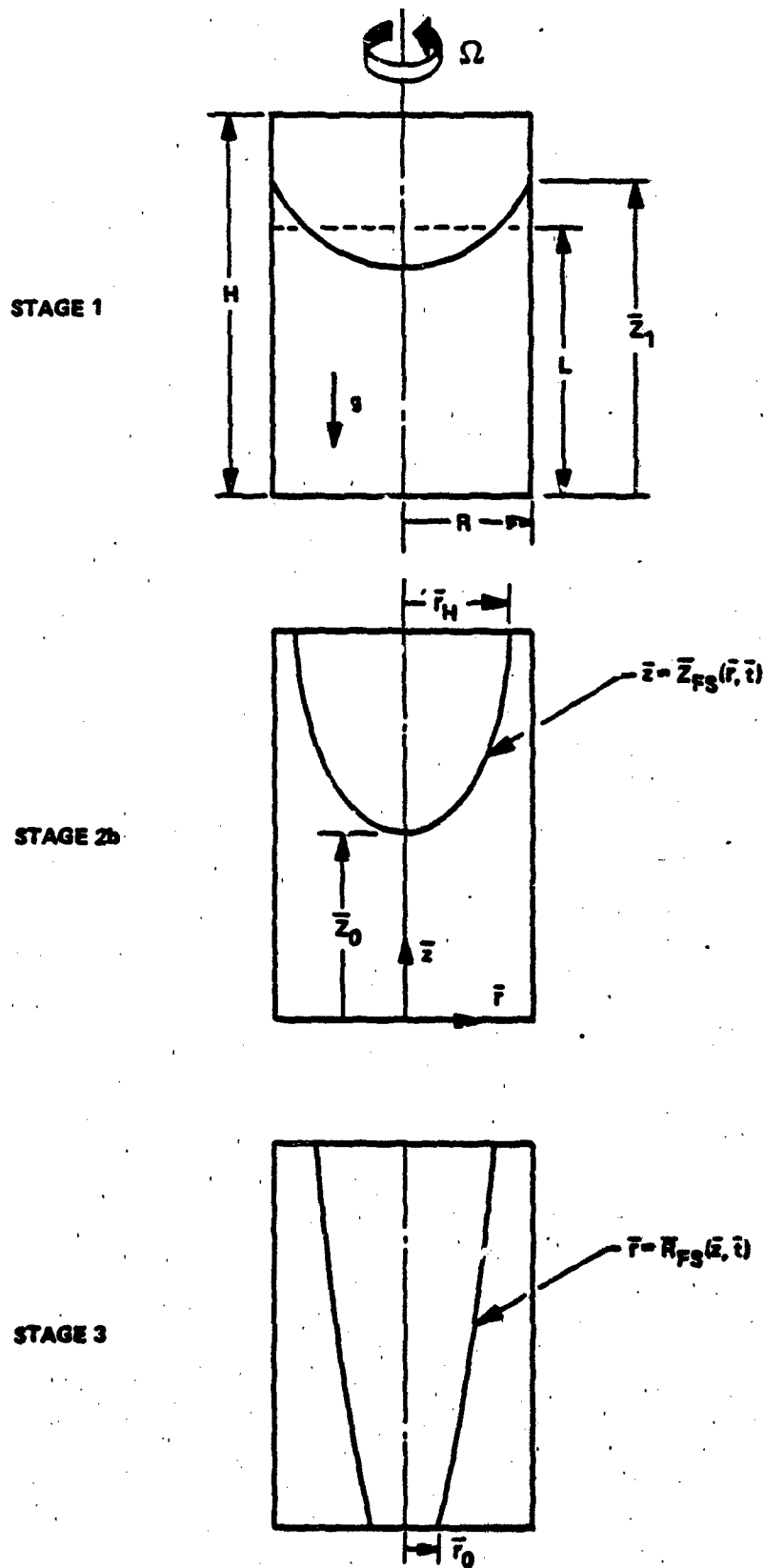


Figure 1 CYLINDRICAL GEOMETRY AND POSSIBLE FLUID CONFIGURATIONS DURING SPIN-UP

at large Reynolds number, the dominant spin-up mechanism is a secondary flow driven by the viscous endwall Ekman layers. This secondary flow redistributes the angular momentum acquired in the Ekman layers over the remaining interior "core" flow, which is relatively inviscid. The characteristic spin-up time, t_s , has been found to scale as $(H/R) Re^{1/2} \Omega^{-1}$ (see Nomenclature for a list of symbol definitions).⁸ For large Re , this is much shorter than the time one would expect based solely on viscous diffusion from the sidewall, t_D , which scales as $Re \Omega^{-1}$.

The great majority of previous investigations dealt with the case where the fluid cavity is completely filled; in practice, however, the shells are often only partially filled. Field data⁹ show that the probability of a projectile experiencing an erratic flight is a strong function of its fill ratio, i.e., the percentage of the cavity volume occupied by fluid. Thus there is an important need to understand the influence of the interior free surface on the spin-up process. Gerber¹⁰ has shown that the final form of this surface, after solid-body rotation is achieved, is a parabola whose shape is determined by the fill ratio and the Froude number, $F = (\Omega R)^2/gH$. Goller and Ranov¹¹ studied how the surface contour evolves in time and its influence on spin-up. They employed a simplified model which extended the partly phenomenological analysis of Wedemeyer¹² for the filled case. Their analysis indicated that the free surface motion acts to retard the spin-up process. Numerical results for both the azimuthal velocity field and the surface contour were obtained as functions of time, and the latter exhibited good agreement with their experimental data. The problem with applying their analysis to actual configurations is that Goller and Ranov assumed the free surface did not intersect either of the endwalls. This is a rather restrictive assumption, as shown by the analysis of Gerber,¹⁰

Accordingly, the goal of the first phase of the present investigation was to extend the simplified Wedemeyer-Goller-Ranov model to situations where the free

8. Greenspan, H.P., The Theory of Rotating Fluids, Cambridge University Press, London, 1968.
9. Mark, A., Measurements of Angular Momentum Transfer in Liquid-Filled Projectiles, ARBRL-TR-2029, Aberdeen Proving Ground, Md., November 1977.
10. Gerber, N., "Properties of Rigidly Rotating Liquids in Closed Partially Filled Cylinders," ASME Transactions, J. of Applied Mechanics, Vol. 97, 734-735, 1975.
11. Goller, H. and Ranov, T., "Unsteady Rotating Flow in a Cylinder with a Free Surface," ASME Transactions, J. of Basic Engineering, Vol. 90D, No. 4, 445-454, December 1968.
12. Wedemeyer, E.H., "The Unsteady Flow Within a Spinning Cylinder," J. of Fluid Mechanics, Vol. 20 Pt. 3, 383-399, 1964.

surface may intersect one or both endwalls. This portion of the work is discussed in Section 2. Unfortunately, there appear to be no data for such flows, either experimental or numerical, against which to compare the simplified model's predictions. So in the second phase of the investigation we undertook the development of a more refined model, based on the full Navier-Stokes equations, which removes the principal approximations of the earlier analysis. The form of the equations and the finite difference algorithm used to solve them are described in Section 3. Section 4 summarizes the conclusions drawn from the investigation and suggests where further work is needed.

2. SIMPLIFIED MODEL

This model has been the subject of an earlier interim report.⁶ Since its preparation, a few improvements have been made, and the revised model and its results are the subject of a manuscript submitted for journal publication.⁷ Hence only a brief summary of the principal approximations and equations will be given here.

2.1 Principal Assumptions and Equations

We wish to predict the spin-up of fluid in a cylinder of radius R and height H (see Fig. 1) which at $t = 0$ impulsively begins to spin with constant angular velocity, Ω , about its axis. The fluid is incompressible and characterized by its density, ρ , and kinematic viscosity, ν . Its initial level when at rest is denoted by L . The velocity components in the (r, θ, z) coordinates are (u, v, w) respectively. Time is here normalized by Ω^{-1} , velocities by ΩR , and the radial and axial dimensions by R and H , respectively.

As noted earlier, the present model builds on the previous investigations of Wedemeyer¹², and Goller and Ranov¹¹. In the fully filled case, Wedemeyer argued that in the limit of large Re the flow could be conceptually divided into two regions: the viscous flow in the endwall Ekman layers, and the so-called "core" flow away from the endwalls where viscous effects are much less important. In this limit, the u and w velocity components are much smaller than the azimuthal component, v , so that most terms in the Navier-Stokes equations involving u and w are neglected. This leads to a simplified model in which u , v and the pressure p are functions of only r and t , the so-called "columnar" flow approximation. The momentum equation governing $v(r, t)$ in the core flow reduces to,

$$\frac{\partial v}{\partial t} + u \left(\frac{\partial v}{\partial r} + \frac{v}{r} \right) = Re^{-1} \left[\frac{\partial^2 v}{\partial r^2} + \frac{\partial}{\partial r} \left(\frac{v}{r} \right) \right] \quad (1)$$

subject to the initial and boundary conditions,

$$v(r, 0) = 0 \quad 0 \leq r \leq 1 \quad (2a)$$

$$v(0, t) = 0 \quad t > 0 \quad (2b)$$

$$v(1, t) = 1 \quad t > 0 \quad (2c)$$

The free surface contour is denoted by $Z_{FS}(r, t)$. Following Goller and Ranov,¹¹ its evolution is governed by an equation which balances the centripetal and gravitational force components tangential to the surface:

$$\frac{dZ_{FS}}{dr} = F \frac{v^2}{r} \quad (3)$$

Equation (1) is solved using a Crank-Nicholson type implicit finite-difference scheme on a uniform radial grid. Equation (3) is then integrated numerically, using a Simpson's rule quadrature, to update the surface contour. Note that Eq. (1) is still nonlinear owing to the presence in the convective term of u , which is itself a function of v . Hence an iterative process is required at each time step to get a consistent solution; the details can be found in Ref. 6.

The relation between u and v is the missing link needed to close the above system. For the filled case, Wedemeyer¹² derived such a relation by arguing that whatever outward radial mass flux is generated in the endwall Ekman layers must be balanced at each radial station by an equal but opposite inward flux in the core flow. The flux in the Ekman layers is known to develop on a time scale very much faster than the spin-up time. Hence its magnitude can be predicted at each instant by assuming that it responds in a quasi-steady manner to changes in the azimuthal velocity of the core flow above it. Since the columnar nature of the flow dictates that the compensating radially inward flux in the core flow be spread uniformly in the axial direction, this gives the needed relation between u and v . It is this inward flux that is responsible for distributing the angular momentum acquired in the endwall layers over the remaining fluid.

The preceding argument gives the contribution to u in the core flow caused by Ekman layer pumping. Goller and Ranov¹¹ reasoned that, in the partially filled case, this would be opposed by an outward flux in the core owing to the fact that fluid is being flung out toward the sidewall and away from the centerline. Specifically, the time rate of change of fluid volume between the centerline and the cylindrical surface at any radius r must equal the flux of fluid across the surface. Again the columnar approximation requires that this be spread uniformly in the axial direction. The result is an expression for the positive contribution to u created by the free surface motion. To the extent that it opposes the negative contribution driven by the Ekman layers, the spin-up process is retarded.

The specific form of the equations for u (v) may be found in Ref. 6 and 7. For flows in which the free surface does not intersect either endwall, the model is essentially the same as Goller and Ranov's. The principal difference is the use here of an implicit, as opposed to their explicit, time-marching algorithm; this was done to allow the use of increased time steps, and hence shorter running times.

The present model departs from that of Goller and Ranov in cases where one or both of the endwalls are intersected by the free surface. Of particular interest is the question of how best to describe the surface contour after both endwalls are intersected. Now both limits of integration in applying Eq. (3) (r_0 and r_H in Fig. 1) become functions of time and the surface contour is very steep; this complicates the accurate integration of Eq. (3) with respect to r . Both difficulties can be overcome by switching to a description of the surface as $R_{FS}(z, t)$, and reinterpreting Eq. (3) with z , rather than r , as the independent variable of integration. With this frame of reference, the contour has a shallow slope and lies between constant limits of integration. The price one pays is that an integral equation must be inverted to obtain $R_{FS}(z, t)$, but this turns out to be amenable to a simple relaxation solution which usually converges in a few iterations. For details, the reader is referred to Refs. 6 and 7.

Another distinguishing feature of the present model is that, once the free surface has intersected an endwall, the Ekman layer there no longer completely wets the surface. To the author's knowledge, there have been no published investigations into the structure of the layer which forms in such a case. Accordingly, heuristic reasoning was used to suggest simple analytical modifications to the Wedemeyer expressions which reflect the expected reduced mass flux, and still remain within the columnar flow approximation. These expressions were quoted in Ref. 6 as Eq. (19) for U_{TEL} and Eq. (25) for U_{BEL} , which represent the contributions to u in the core flow from the top and bottom Ekman layers, respectively.

2.2 Modifications To Original Model

Subsequent to the preparation of Ref. 6, modifications were made to the analysis to better reflect the physical phenomena. One of these changes has to do with the heuristic modeling of the Ekman layer pumping from a partially wetted surface, as just described above. The expression now used for the contribution to u from the layer on the top endwall is:

$$u_{TEL} = 0 \quad 0 \leq r \leq r_H \quad (4a)$$

$$u_{TEL} = -K_E^{-\frac{1}{2}} (R/H) r K_T (1 - r_H/r)^{\delta_T} f(\omega) \quad r_H \leq r \leq 1 \quad (4b)$$

which replaces Eq. (19) of Ref. 6. Here $r_H(t)$ is the radius at which the top wall is intersected by the free surface, and K_T and δ_T are adjustable constants. The quantity $f(\omega)$ represents the dimensionless mass flux integral appearing in the Wedemeyer¹² model, as a function of the local angular velocity, $\omega = v/r$ (see Eq. (10) of Ref. 6).

This expression satisfies the following constraints: u remains continuous across $r = r_H$; the contribution from u_{TEL} vanishes at both $r = r_H$ and 1, as it should; the influence of the top endwall Ekman layer will increase as r_H decreases, which is intuitively satisfying; and the columnar nature of the flow is maintained. It also reduces to the form of the original Wedemeyer model in the fully filled limit, $r_H = 0$; this last point was not true of Eq. (19) in Ref. 6. Practically speaking, however, this change had a negligible influence on the numerical results for the conditions studied here.

An expression analogous to Eq. (4) above was used for u_{BEL} , and satisfies similar criteria (Eq. (25) of Ref. 6). Certainly other analytical forms can be found which would satisfy these constraints. But in the absence of any experimental data to serve as a guide, it was decided to employ as simple a form as possible.

Another modification to the original model concerns the appropriate boundary condition to apply to Eq. (1) once a portion of the bottom wall is exposed. After this occurs, one cannot expect Eq. (2b) to apply, as there is no longer any fluid at the axis. At the contact line, $r = r_0$ in Fig. 1, one is faced with the apparently conflicting requirements that there be no slip at the solid surface, but that the contact line nevertheless be allowed to move. The resolution of this paradox is still an active area of research, see e.g., Ref. 13, but beyond the scope of the present investigation. In our simplified model we initially chose to use a no-slip condition, viz. $v(r_0) = r_0$ (Ref. 6). This produced a discontinuous change in angular velocity near the origin as the free surface passed through this point. An argument can also be made that one has no right to impose a no-slip condition on the (relatively) inviscid core flow described

-
13. Pismen, L.M. and Nir, A., "Motion of a Contact Line," *Physics of Fluids*, Vol. 25, No. 1, 3-7, January 1982.

by Eq. (1), where the terms needed to define the Ekman layer structure have already been eliminated.

Accordingly, an alternative boundary condition on $v(r_0)$ is now used, one based on the kinematic condition that a particle on the free surface must remain there. It is most easily derived by taking the integral of Eq. (3) from r_0 to some general position r , differentiating the result with respect to time, and then evaluating it at $r = r_0(t)$. The boundary condition one obtains is:

$$v(r_0) = \left[\frac{-r_0 \partial Z_{FS}(r_0, t) / \partial t}{F dr_0 / dt} \right]^{1/2} \quad (5)$$

which replaces Eq. (20) of Ref. 6.

2.3 Results

After changing the analysis as described in Section 2.2, the numerical results presented in Ref. 6 were rerun with the modified code. These include cases for a range of Froude number, Reynolds number, and fill ratio. The revised results are presented in Ref. 7. A representative sample case is displayed here in Fig. 2. This is referred to as Case 3 in Ref. 6 and 7 and corresponds to $Re = 1.172 \times 10^5$, $F = 3.5$, $H/R = 3.0$, and $L/H = 0.6$. The azimuthal velocity profiles vs. radius are shown in Fig. 2a. The first nine profiles are for dimensionless times $t = 400$ to 3600 in increments of 400 . The last profile, for $t_s = 4745$, integrates to a total angular momentum about the axis greater than 99% of its final value, at which point the calculation was stopped. The fluid then is for all practical purposes in solid-body rotation. The last five profiles in Fig. 2a end abruptly on the left end at the point $r = r_0(t)$, where the free surface has intersected the bottom wall. Since there is no fluid to the left of this point, v is undefined there.

This is more clearly seen in Fig. 2b, which shows the free surface profiles for the same times. The asymptotic nature of the approach to solid-body rotation is evident in both figures from the closer spacing of the profiles later in the calculation. Note also that the surface contours become quite steep, and thus warrant the extra effort spent in switching from a radial to an axial grid for the surface integrals when both endwalls are intersected.

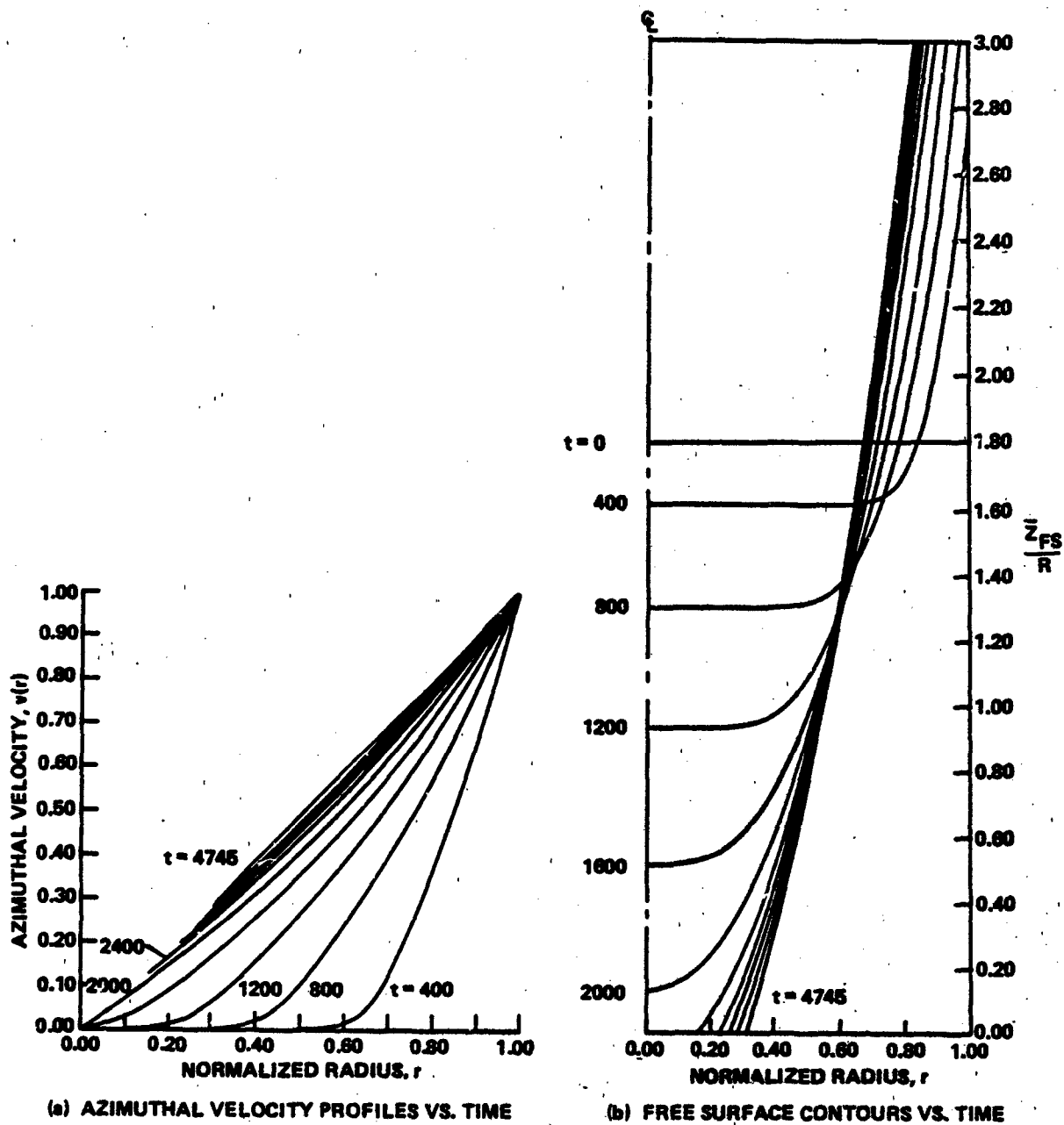


Figure 2 NUMERICAL RESULTS FOR CASE 3 (FROM REF. 7)

A semi-logarithmic plot of the dimensionless angular momentum deficit, $1-L_z(t)/L_z(\infty)$, vs. $Re^{-1/2}t$ is presented for Case 3 in Fig. 3. The reason for scaling the time axis in this way is because linearized analysis indicates that the dimensionless spin-up time scales as $Re^{1/2}$ (Ref. 8). For comparison purposes, the results from Cases 4 and 5 (Ref. 7) are also presented on this plot; these cases differ from Case 3 only in the values chosen for Re , which are indicated on the figure. For each case two flagged symbols are shown. The first of these represents the instant at which the free surface first hits the top wall; the second, the instant at which it intersects the bottom wall.

The most noteworthy feature of Fig. 3 is that up to the instant where the bottom wall is intercepted, the data in each case lie on a straight line. This is consistent with the finding of linearized theory for the fully filled case that the time dependence of the spin-up process is a simple exponential. What is surprising is the degree to which this remains true here, where nonlinearities and a free surface are both present. After the bottom endwall is intercepted, however, the numerical data in Fig. 3 follow a line with a reduced slope, indicating a slower rate of spin-up.

The fact that the surface hitting the top wall apparently has little effect on the rate of spin-up can be explained by noting that the radial extent of the fluid at the top wall in Fig. 2b is relatively thin; moreover, the fluid in this region has already acquired a significant fraction of its final angular velocity. Hence its contribution to the Ekman pumping remains small compared with that from the bottom layer, which still completely covers the wall. Once the bottom wall is intercepted in the final stage, however, the strength of the bottom Ekman layer pumping is progressively reduced as the wall is exposed, and a slower spin-up rate results. Thus, it is the bottom Ekman layer which is the dominant driving force behind the secondary flow responsible for spin-up.

As noted in Section 2.2, Cases 3-5 had originally been run (Ref. 6) with a no-slip condition on $v(r_0)$, whereas the results reported here and in Ref. 7 used Eq. (5). A comparison of the two sets of results shows that the latter lowers the velocity profiles in the immediate vicinity of r_0 , and increases the spin-up time by 3%, 5% and 19% for Cases 3-5, respectively. Referring again to Fig. 3, the only qualitative change of any note was that, with the no-slip condition, Case 5 had previously exhibited no kink as the bottom wall was intersected. This was interpreted as meaning the Reynolds number in this case was low enough for viscous diffusion from the sidewall to dominate

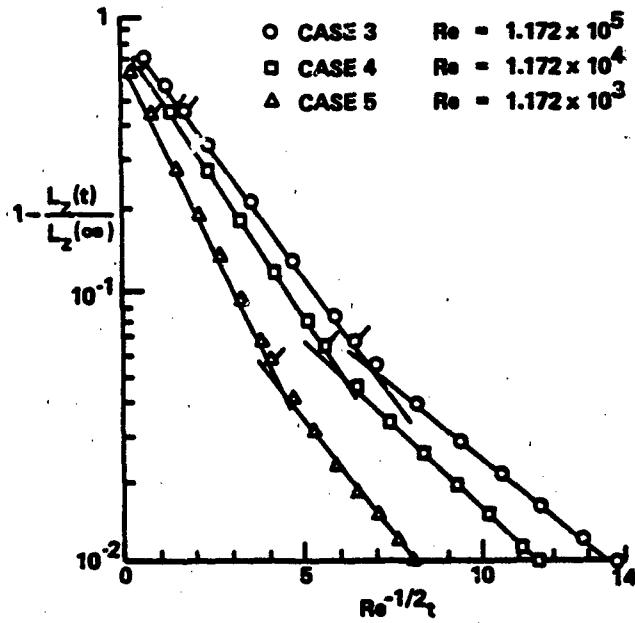


Figure 3 ANGULAR MOMENTUM DEFICIT VS. TIME FOR CASES 3 THRU 5 (FROM REF. 7)

over Ekman layer pumping. With the revised results all that can be said is that the change in rate of spin-up at the second transition decreases with decreasing Re in Fig. 3. Finally, it is interesting to note that the angular momentum ratios at the times at which transitions occur are nearly independent of Re .

Additional numerical results and discussion may be found in Refs. 6 and 7.

3. NAVIER-STOKES MODEL

The simplified model described in the preceding section is predicated on the following principal approximations: conceptual division of the flow into the viscous endwall Ekman layers, and the relatively inviscid "core" flow; the assumption of columnar flow in the core; and the quasi-steady treatment of the Ekman layer pumping. Each of these becomes more questionable as the Reynolds number is lowered. Moreover, the only experimental data available to validate the simplified model's predictions are those in Ref. 11, which pertain only to situations where the free surface intersects neither of the endwalls.

Hence the goal of the second phase of the present program, described below, was to develop a more refined numerical model based on the full Navier-Stokes equations. Such a model would relax all the above assumptions, and serve to validate over what range of parameters the simplified model could be trusted.

3.1 Governing Equations

The flow in principle is governed by the continuity equation,

$$\nabla \cdot \vec{v} = 0 \quad (6)$$

and the Navier-Stokes equations,

$$\frac{\partial \vec{v}}{\partial t} + \nabla \cdot (\vec{v} \vec{v}) = -\nabla p - F^{-1} \frac{R}{H} \hat{k} - Re^{-1} \nabla \times \nabla \times \vec{v} \quad (7)$$

where the time t is again normalized by Ω^{-1} , the velocities by ΩR , and the pressure by $\rho(\Omega R)^2$. In contrast to the simplified model, however, all lengths are here normalized by the cylinder radius, R . In dimensionless coordinates then, the cylinder maps to the region $0 \leq r \leq 1$, $0 \leq z \leq H/R$.

The convective term in Eq. (7) has been written in conservative form using the identity

$$\vec{v} \cdot \nabla \vec{v} = \nabla \cdot (\vec{v} \vec{v}) - \vec{v} (\nabla \cdot \vec{v})$$

while the viscous term was transformed using

$$\nabla^2 \vec{v} = -\nabla \times (\nabla \times \vec{v}) + \nabla (\nabla \cdot \vec{v})$$

The second term in each identity vanishes as required by Eq. (6), and the result is Eq. (7). In this form the finite difference analog of the convective terms conserves momentum. The reason for transforming the viscous terms in this way will become apparent shortly.

Equations (6) and (7) comprise four scalar equations for the unknowns u , v , w and p . An additional relation is needed to predict the unknown free surface contour. As before, we describe the free surface by $G = z - Z_{FS}(r, t) = 0$. The kinematic condition that a fluid particle on the surface must remain there then requires that ¹⁴

$$\frac{DG}{Dt} = \frac{\partial G}{\partial t} + \vec{v} \cdot \nabla G = 0 \quad (8)$$

at the surface, $G = 0$.

When written out in cylindrical coordinates, Eqs. (6) - (8) become

$$\frac{1}{r} \frac{\partial(ru)}{\partial r} + \frac{\partial w}{\partial z} = 0 \quad (6)$$

$$\begin{aligned} \frac{\partial u}{\partial t} = & - \left[\frac{1}{r} \frac{\partial(ru^2)}{\partial r} - \frac{u^2}{r} + \frac{\partial(uw)}{\partial z} \right] - \frac{\partial p}{\partial r} \\ & + Re^{-1} \frac{\partial}{\partial z} \left[\frac{\partial u}{\partial z} - \frac{\partial w}{\partial r} \right] \end{aligned} \quad (7a)$$

$$\begin{aligned} \frac{\partial v}{\partial t} = & - \left[\frac{\partial(ruv)}{\partial r} + \frac{uv}{r} + \frac{\partial(wv)}{\partial z} \right] \\ & + Re^{-1} \left\{ \frac{\partial}{\partial r} \left[\frac{1}{r} \frac{\partial(rv)}{\partial r} \right] + \frac{\partial^2 v}{\partial z^2} \right\} \end{aligned} \quad (7b)$$

$$\begin{aligned} \frac{\partial w}{\partial t} = & - \left[\frac{\partial w^2}{\partial z} + \frac{1}{r} \frac{\partial(ruw)}{\partial r} \right] - \frac{\partial p}{\partial z} - F^{-1} \frac{R}{H} \\ & + Re^{-1} \frac{1}{r} \frac{\partial}{\partial r} \left[r \left(\frac{\partial w}{\partial r} - \frac{\partial u}{\partial z} \right) \right] \end{aligned} \quad (7c)$$

14. Batchelor, G.K., An Introduction to Fluid Dynamics, Cambridge University Press, 1967.

$$\frac{\partial Z_{FS}}{\partial t} = \omega_{FS} - u_{FS} \frac{\partial Z_{FS}}{\partial r} \quad (8)$$

where, e.g., w_{FS} represents the axial velocity component at a point on the free surface. The only assumptions that have been made in writing the above equations are that the flow remains axisymmetric and laminar.

To uniquely define the problem, initial and boundary conditions for Eqs. (6) - (8) are needed. They are most easily discussed below in connection with the finite difference form of the equations.

3.2 Coordinate Transformations

In order to better resolve the viscous Ekman layers on the endwalls and the Stewartson layer at the sidewall, a coordinate stretching is employed. We use the same transformation successfully used by Kitchens¹⁵ for the filled case. The radial coordinate r is transformed to ρ where

$$\rho = \ln \left(\frac{b+r}{b-r} \right) / \ln \left(\frac{b+1}{b-1} \right) \quad (9a)$$

The inverse transformation is

$$r = b \left[\left(\frac{b+1}{b-1} \right)^\rho - 1 \right] / \left[\left(\frac{b+1}{b-1} \right)^\rho + 1 \right] \quad (9b)$$

15. Kitchens, C.W., Jr., "Navier-Stokes Solutions for Spin-Up in a Filled Cylinder," AIAA J., Vol. 18, No. 8, 929-934, August 1980.

Similarly, the axial coordinate is transformed according to

$$\xi = \frac{1}{2} + \frac{1}{2} \ln \left(\frac{c + \frac{2R}{H} z - 1}{c - \frac{2R}{H} z + 1} \right) / \ln \left(\frac{c+1}{c-1} \right) \quad (10a)$$

whose inverse is given by,

$$z = \left(\frac{H}{2R} \right) (c-1) \left[\left(\frac{c+1}{c-1} \right)^{2\xi} - 1 \right] / \left[1 + \left(\frac{c+1}{c-1} \right)^{2\xi-1} \right] \quad (10b)$$

The above transformations map the cylinder into the unit square $0 \leq \rho \leq 1$, $0 \leq \xi \leq 1$ in the (ρ, ξ) computational plane. The constants b and c (≥ 1) are input parameters used to adjust the grid spacing; as b and c approach unity from above, progressively more points will be clustered near the side- and endwalls in the physical (r, z) plane, respectively.

Upon application of the above transformations, Eqs. (6)-(8) become, in the computational plane:

$$r^{-1} \rho_r (r u)_\rho + \xi_z \omega_\xi = 0 \quad (11)$$

$$u_\xi = - \left[r^{-1} \rho_r (r u^2)_\rho - r^{-1} v^2 + \xi_z (u \omega)_\xi \right] - \rho_r \rho_\rho + R e^{-1} \xi_z [\xi_z u_\xi - \rho_r \omega_\rho]_\xi \quad (12a)$$

$$v_\xi = - \left[r^{-1} \rho_r (r u v)_\rho + r^{-1} u v + \xi_z (\omega v)_\xi \right] + R e^{-1} \left[\rho_r (r^{-1} \rho_r (r v)_\rho)_\rho + \xi_z (\xi_z v_\xi)_\xi \right] \quad (12b)$$

$$\begin{aligned} \omega_t = & - r^{-1} \rho_r (r u \omega)_\rho + \xi_z (\omega^2)_\xi - \xi_z \rho_\xi - \left(\frac{F H}{R} \right)^{-1} \\ & + Re^{-1} r^{-1} \rho_r \left[r (\rho_r \omega_\rho - \xi_z u_\xi) \right]_\rho \end{aligned} \quad (12c)$$

$$(Z_{FS})_t = \omega_{FS} - u_{FS} \rho_r (Z_{FS})_\rho \quad (13)$$

where subscripts are used to denote differentiation.

3.3 Computational Grid

The above equations are differenced on a uniform rectangular grid in the computational (ρ, ξ) plane. Initially an attempt was made to use a conventional grid, i.e. one in which the velocity components and pressure are all defined at the same grid locations. But it was found that this leads to an inconsistency between the difference forms of the velocity and pressure equations. This will be mentioned again below in connection with the form of those equations.

The differencing scheme now used employs a so-called "staggered" or interlocking grid, which was first proposed by Welch, et al.¹⁶ in connection with the Marker-and-Cell (MAC) method. Although the explicit MAC method is not used here, for incompressible flows the staggered grid arrangement still has clear advantages. This arrangement is shown in Fig. 4. The letters j and k are used as indices in the radial and axial coordinates, respectively. The pressure p is defined at the center of each grid cell, $p_{j, k}$, i.e. where integral values of j and k intersect. The radial and azimuthal velocities are defined at the center of the cell's vertical faces, at $(j \pm 1/2, k)$; and the axial velocity is defined at the center of the horizontal faces, at $(j, k \pm 1/2)$.

16. Welch, J.E., Harlow, F.E., Shannon, J.P. and Daly, B.J., The MAC Method: A Computing Technique for Solving Viscous, Incompressible, Transient Fluid-Flow Problems Involving Free Surfaces, Los Alamos Scientific Laboratory Report LA-3425, March 1966.

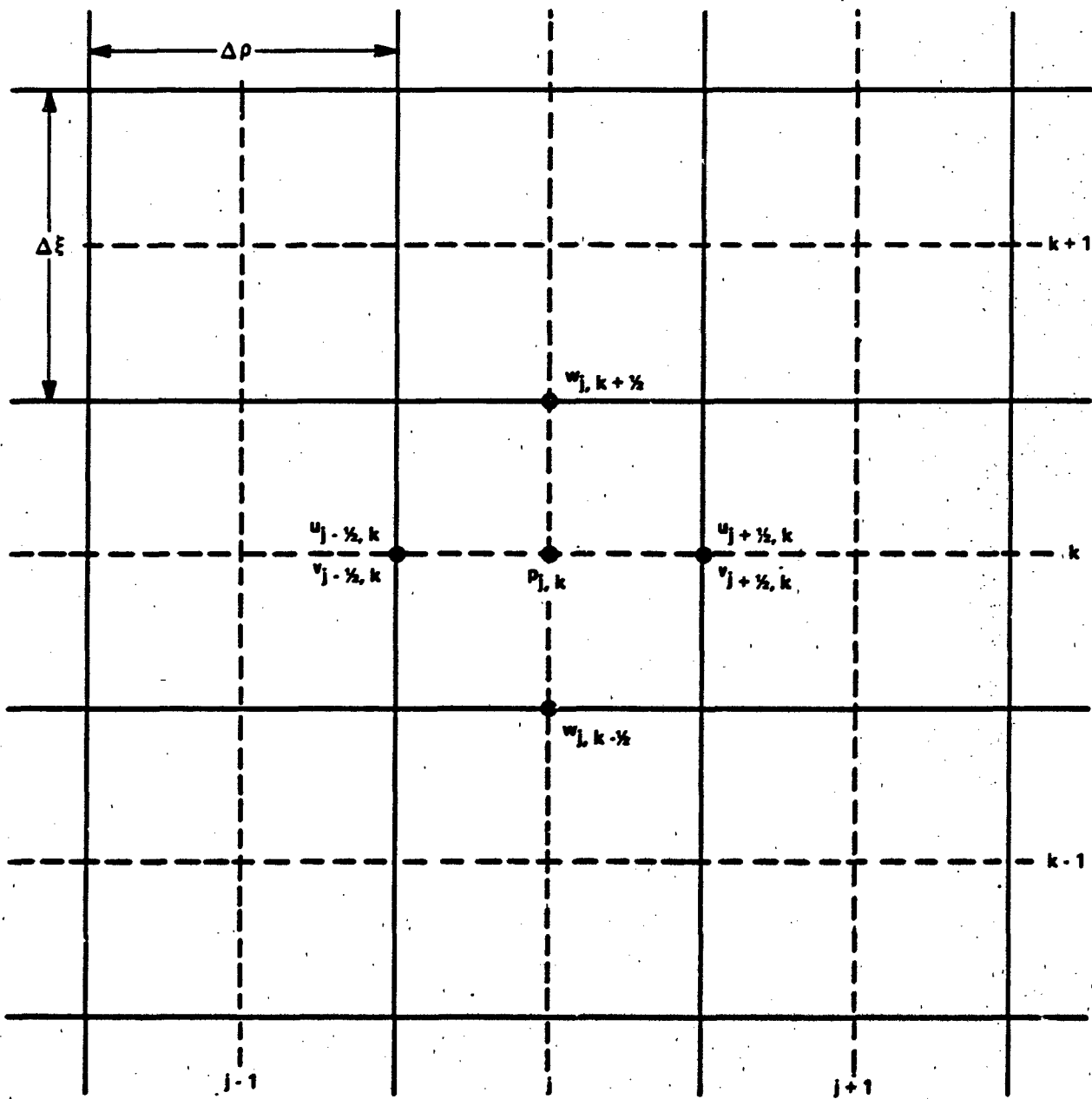


Figure 4 STAGGERED GRID ARRANGEMENT

The grid is numbered in such a way that the cylinder axis and the sidewall lie along $j = 3/2$ and $j = NJ - 1/2$, respectively; NJ is the chosen number of radial grid cells. The relation between ρ and j is thus $\rho = (j - 3/2) \Delta\rho$, where $\Delta\rho = 1/(NJ-2)$. Analogously, the bottom and top endwalls lie along $k = 3/2$ and $k = NK - 1/2$, respectively, with NK the number of axial cells. Thus $\xi = (k - 3/2) \Delta\xi$, where $\Delta\xi = 1/(NK-2)$.

3.4 Difference Equations For Velocities

The algorithm used to solve the equations is an adaptation of the semi-implicit Predictor-Corrector Multiple-Iteration (PCMI) method. This method was first proposed by Rubin and Lin¹⁷ for solving steady, three-dimensional boundary layer problems. Kitchens¹⁵ used it to study the spin-up problem in a filled cylinder, which is believed to be the method's first application to the full, unsteady Navier-Stokes equations. Because of the absence of a free surface, Kitchens was able to more easily formulate his equations in terms of the stream function-vorticity variables. The present study is thus believed to be the first time the PCMI scheme has been applied to the primitive variable formulation of the Navier-Stokes equations, with a free surface present.

The basic idea of the PCMI scheme is rather simple. We will use a uniform time step, Δt , and a superscript i to denote the time level such that $t = i \Delta t$. At the beginning of the step to time $(i + 1)$, all flow variables at level i will be known. The first "predictor" part of the calculation consists of extrapolating all flow variables to level $(i + 1)$ using information from the three previous levels:

$$Y^{i+1} = 3Y^i - 3Y^{i-1} + Y^{i-2} \quad (14)$$

which is accurate to order $(\Delta t)^3$. Here Y is a generic symbol for u , v or w , and spatial indices have been dropped for simplicity. For the first two time steps, extrapolations of order Δt and $(\Delta t)^2$ are used, respectively. Equation (14) provides starting values for each of the variables. This is followed by an iterative process in which solution of the Navier-Stokes equations serves to "correct" the initial guess.

17. Rubin, S. G. and Lin, T. C., "A Numerical Method for Three-Dimensional Viscous Flow: Application to the Hypersonic Leading Edge," *J. of Computational Physics*, Vol. 9, 339-364, 1972.

The time derivative in Eq. (12) is approximated at level $(i + 1)$ by second-order backward differences,

$$Y_t^{i+1} = (3Y^{i+1} - 4Y^i + Y^{i-1}) / 2 \Delta t$$

For consistency, the spatial derivatives on the right side of Eq. (12) must also be evaluated at $(i+1)$, hence the implicit nature of the scheme. For example, let $u_{j+\frac{1}{2},k}^{n+1}$ denote the $(n + 1)$ iterate to the desired $u_{j+\frac{1}{2},k}^{i+1}$. The viscous and pressure gradient terms are then approximated by second-order centered differences. Derivatives in the ρ coordinate are treated implicitly, i.e. in terms of $(n + 1)$ iterate values. Derivatives in the ξ direction use these values as they become available, with (n) iterate values used where they are not, as the grid is swept from bottom to top. For example, the viscous terms in Eq. (12a) are approximated by

$$\begin{aligned} & [Re^{-1} \xi_x (\xi_x u_x - \rho_r \omega_\rho)]_{j+\frac{1}{2},k}^{i+1} \\ & \approx Re^{-1} \left(\frac{\xi_x}{\Delta \xi} \right)_k \left[\left(\frac{\xi_x}{\Delta \xi} \right)_{k+\frac{1}{2}} (u_{j+\frac{1}{2},k+1}^n - u_{j+\frac{1}{2},k}^{n+1}) - \left(\frac{\rho_r}{\Delta \rho} \right)_{j+\frac{1}{2}} (\omega_{j+1,k+\frac{1}{2}}^n - \omega_{j,k+\frac{1}{2}}^n) \right. \\ & \quad \left. - \left(\frac{\xi_x}{\Delta \xi} \right)_{k-\frac{1}{2}} (u_{j+\frac{1}{2},k}^{n+1} - u_{j+\frac{1}{2},k-1}^n) + \left(\frac{\rho_r}{\Delta \rho} \right)_{j+\frac{1}{2}} (\omega_{j+1,k-\frac{1}{2}}^{n+1} - \omega_{j,k-\frac{1}{2}}^n) \right] \end{aligned}$$

The nonlinear convective terms in the equations are differenced using a hybrid of centered and upwind schemes, as suggested by Hirt, et al.¹⁸ As an example, the radial convection term in Eq. (12a) becomes

18. Hirt, C.W., Nichols, B.D. and Romero, N.C., SOLA - A Numerical Solution Algorithm for Transient Fluid Flows, Los Alamos Scientific Laboratory Report LA-5852, April 1975.

$$\begin{aligned}
& \left[-r^{-1} \rho_r (ru^2)_\rho \right]_{j+\frac{1}{2},k}^{i+1} \\
& \approx \frac{1}{r_{j+\frac{1}{2}}} \left(\frac{\rho_r}{\Delta \rho} \right)_{j+\frac{1}{2}} \left\{ r_{j+1} \left[u_{j+1,k}^n u_{j+1,k}^{n+1} + \frac{\alpha}{2} |u_{j+1,k}^n| (u_{j+\frac{1}{2},k}^{n+1} - u_{j+\frac{3}{2},k}^{n+1}) \right] \right. \\
& \quad \left. - r_j \left[u_{j,k}^n u_{j,k}^{n+1} + \frac{\alpha}{2} |u_{j,k}^n| (u_{j-\frac{1}{2},k}^{n+1} - u_{j+\frac{1}{2},k}^{n+1}) \right] \right\}
\end{aligned}$$

where α is an adjustable input parameter between zero and one. For $\alpha = 0$, centered differencing is recovered, while $\alpha = 1$ yields full upwind or "donor-cell" differencing.¹⁹ Such a scheme is stable and conservative, yet reduces the formal truncation error to first-order; as pointed out in Refs. 19 and 20, it may still produce results comparable in accuracy to those of a second-order centered scheme. Note that the convective velocity is evaluated from the previous iterate, so that the algebraic equations are rendered linear. The above form calls for values of u and w which are not defined in the grid system of Fig. 4. For such quantities, simple averages are taken, e.g.,

$$u_{j,k} = \frac{1}{2} (u_{j-\frac{1}{2},k} + u_{j+\frac{1}{2},k})$$

This scheme leads to a tridiagonal system of equations for each of the velocity components along a given k row. Because of their length, the full system is given in the Appendix. For each k , the equations are easily solved using a standard algorithm for inverting tridiagonal systems.¹⁹ The initial conditions at $t = 0$ are $u = v = w = 0$ everywhere. The grid is swept by first correcting the values adjacent to the endwall, $k = 2$, and proceeding one row at a time up to the free surface.

At the cylinder axis, the following boundary conditions are imposed:

$$\begin{aligned}
u_{\frac{1}{2},k} &= v_{\frac{1}{2},k} = 0 \\
w_{1,k+\frac{1}{2}} &= w_{2,k+\frac{1}{2}}
\end{aligned} \tag{15}$$

-
19. Roache, P.J., Computational Fluid Dynamics, Hermosa Publishers, Albuquerque, N.M., 1976.
 20. Spalding, D. B., "A Novel Finite Difference Formulation for Differential Expressions Involving both First and Second Derivatives," International Journal for Numerical Methods in Engineering, Vol. 4, 551-559, 1972.

At the bottom wall, a no-slip condition is enforced:

$$\begin{aligned} u_{j+\frac{1}{2},1} &= -u_{j+\frac{1}{2},2} \\ v_{j+\frac{1}{2},1} &= 2\tilde{\Omega}r_{j+\frac{1}{2}} - v_{j+\frac{1}{2},2} \\ \omega_{j,\frac{3}{2}} &= 0 \end{aligned} \quad (16)$$

And at the sidewall, the following obtain:

$$\begin{aligned} u_{NJ-\frac{1}{2},k} &= 0 \\ v_{NJ-\frac{1}{2},k} &= \tilde{\Omega} \\ \omega_{NJ,k+\frac{1}{2}} &= -\omega_{NJ-1,k+\frac{1}{2}} \end{aligned} \quad (17)$$

where $\tilde{\Omega}$ denotes the cylinder's angular velocity normalized by its final value. For ideally impulsive spin-up, $\tilde{\Omega} = 1$ for $t > 0$. The code allows for a "ramped" imposition of this boundary condition, i.e.,

$$\begin{aligned} \tilde{\Omega} &= t/t_{IMP} & t \leq t_{IMP} \\ \tilde{\Omega} &= 1 & t \geq t_{IMP} \end{aligned} \quad (18)$$

where typically $t_{IMP} = 10$. Equations (15) - (17) are accurate to second order.

Finally, there is the question of what boundary conditions are appropriate at the free surface. Let $KT(j)$ denote the topmost cell in the j -column which contains fluid. Following Hirt, et al.¹⁸ if $KT(j)$ does not exceed $KT(j-1)$ the azimuthal and radial velocities at $(j+1/2, KT)$, along with all other interior cell values to their right, are corrected via the Navier-Stokes equations as described above; otherwise, they are set equal to the values in the cell immediately below. In either case, the axial velocity in the surface cells is chosen so as to satisfy the difference approximation to Eq. (11), i.e.,

$$\omega_{j,KT+\frac{1}{2}} = \omega_{j,KT-\frac{1}{2}} - \left(\frac{\xi_z}{\Delta\xi}\right)_{KT}^{-1} r_j^{-1} \left(\frac{\rho_c}{\Delta\rho}\right)_j (r_{j+\frac{1}{2}} u_{j+\frac{1}{2},KT} - r_{j-\frac{1}{2}} u_{j-\frac{1}{2},KT}) \quad (19)$$

This specification assures that the divergence in cell (j, kT) vanishes (see Eq. (20) below).

The above boundary conditions apply to situations in which neither endwall is intersected by the surface, and will require some modification for cases in which this is not so.

The semi-implicit PCMI method described above was chosen over simpler explicit schemes, e.g. the MAC method,¹⁶ for several reasons. Since radial variations are treated implicitly, the allowable Δt depends only on the axial, and not the radial, grid spacing (Refs. 15, 17). Axial gradients in the core flow tend to be much smaller (recall the columnar flow approximation in Section 2), and so will allow larger grid spacings and time steps. Indeed, this is the reason for treating the radial and axial variations implicitly and explicitly, respectively. The PCMI method has also been proven capable of handling the strong nonlinear coupling between the equations, as demonstrated by its success for the filled cylinder problem.¹⁵ Finally, the iterative structure of the scheme provides a convenient framework for correcting the free surface contour at each step. The overall iterative process will be discussed in Section 3.7.

3.5 Difference Equation For Pressure

The time derivative of p does not appear in Eqs. (11)-(13). Hence they cannot be used to march the pressure field forward in time in the same manner as the velocity field. Instead, the pressure field is adjusted at each time step so as to enforce the incompressibility condition expressed by Eq. (11). Let $D = \nabla \cdot \vec{v}$, and $D_{j,k}$ denote its value at the point (j, k) in Fig. 4. Using centered differences,

$$D_{j,k} = r_j^{-1} \left(\frac{\rho r}{\Delta \rho} \right)_j \left(r_{j+\frac{1}{2}} u_{j+\frac{1}{2},k} - r_{j-\frac{1}{2}} u_{j-\frac{1}{2},k} \right) + \left(\frac{\xi z}{\Delta \xi} \right)_k \left(w_{j,k+\frac{1}{2}} - w_{j,k-\frac{1}{2}} \right) = 0 \quad (20)$$

The equation for p is obtained by taking the same linear combination of Eqs. (A-1) and (A-3) as appears in Eq. (20). One can see by inspection that the terms involving time derivatives will lead to:

$$\frac{3D_{j,k}^{i+1} - 4D_{j,k}^i + D_{j,k}^{i-1}}{2\Delta t} \quad (21)$$

which is a second-order accurate approximation to $\left(\frac{\partial p}{\partial t}\right)_{j,k}^{i+1}$

Those terms involving p combine to yield

$$r_j^{-1} \left(\frac{\rho_r}{\Delta \rho}\right)_j \left[r_{j+\frac{1}{2}} \left(\frac{\rho_r}{\Delta \rho}\right)_{j+\frac{1}{2}} (p_{j+\frac{1}{2},k}^{i+1} - p_{j,k}^{i+1}) - r_{j-\frac{1}{2}} \left(\frac{\rho_r}{\Delta \rho}\right)_{j-\frac{1}{2}} (p_{j,k}^{i+1} - p_{j-\frac{1}{2},k}^{i+1}) \right] \\ + \left(\frac{\xi_z}{\Delta \xi}\right)_k \left[\left(\frac{\xi_z}{\Delta \xi}\right)_{k+\frac{1}{2}} (p_{j,k+\frac{1}{2}}^{i+1} - p_{j,k}^{i+1}) - \left(\frac{\xi_z}{\Delta \xi}\right)_{k-\frac{1}{2}} (p_{j,k}^{i+1} - p_{j,k-\frac{1}{2}}^{i+1}) \right]$$

which is a second-order approximation to the Laplacian,

$$\frac{1}{r} \frac{\partial}{\partial r} \left(r \frac{\partial p}{\partial r} \right) + \frac{\partial^2 p}{\partial z^2} = r^{-1} \rho_r (r \rho_r p_r)_r + \xi_z (\xi_z p_z)_z$$

centered at (j, k) . The terms which result from the convection terms in the momentum equations are too lengthy to quote here in their original form. However, they are easily recognized as the difference approximation to the continuum term, $\nabla \cdot (\nabla \cdot \vec{v} \vec{v})$ at (j, k) . This brings up another important point which differentiates the present scheme from the MAC method. One can easily show, using tensor notation and the Einstein summation convention, that

$$\begin{aligned} \nabla \cdot (\nabla \cdot \vec{v} \vec{v}) &= \frac{\partial^2 (v_i v_j)}{\partial x_i \partial x_j} \\ &= v_i \frac{\partial^2 v_i}{\partial x_i \partial x_j} + \frac{\partial v_i}{\partial x_i} \frac{\partial v_j}{\partial x_j} + \frac{\partial v_j}{\partial x_i} \frac{\partial v_i}{\partial x_j} + v_j \frac{\partial^2 v_j}{\partial x_i \partial x_j} \\ &= \frac{\partial v_j}{\partial x_i} \frac{\partial v_i}{\partial x_j} + 2 \vec{v} \cdot \nabla D + D^2 \end{aligned}$$

The last two terms vanish for the continuum equations, as per Eq. (6). In the explicit MAC method, all three terms are essentially included in the pressure equation in difference form. But because they get evaluated at the previous time step, for which $D_{j,k} = 0$ is already satisfied to some prescribed accuracy, the contribution from the last two terms on the right is made vanishingly small - as it should be.

In the present implicit formulation these terms are now evaluated at the new time. However, $D_{j,k}$ in general will not be small during the iteration process prior to convergence, and so the presence of the last two terms on the right can be destabilizing. For this reason, and to be consistent with setting $D_{j,k}^{i+1} = 0$ in the time derivative (see below), we omit the last two terms on the right from the pressure equation. Thus the cylindrical coordinate representation of $\frac{\partial v_j}{\partial x_i} \frac{\partial v_i}{\partial x_j}$ is all that remains of the convective terms. The full difference equation for p is quoted in the Appendix as Eq. (A-4).

By making the above term-by-term identifications, we see that the substitution of Eqs. (A-1) and (A-3) into Eq. (20) yields exactly the same difference equation as would be obtained by first taking the divergence of Eq. (7),

$$\nabla^2 p = -\frac{\partial D}{\partial t} - \nabla \cdot (\nabla \cdot \vec{v} \vec{v})$$

and then applying the difference approximations. At first reading, this statement might appear obvious. But in fact, as discussed by Welch, et al.,¹⁶ the staggered grid arrangement of Fig. 4 appears to be the only one for which this statement is true. In particular, it is not true for a conventional grid arrangement, for which the two approaches produce entirely different results. It was because of just this inconsistency that the conventional grid was abandoned here in favor of the staggered grid (cf. Section 3.3).

Another noteworthy feature of Eq. (A-4) is the complete absence of any viscous terms, which turn out to be self-cancelling. This is the reason for having expressed the viscous terms in the form used in Eq. (7). Since the divergence of the curl of any vector field is identically zero, a considerable simplification of the pressure equation results.

Equation (A-4) recognizes that while D is supposed to vanish throughout the flow at all time steps, because we can never solve the equations exactly some small but finite divergence will be present in the solutions at times i and (i-1). However, the pressure field is now to be determined in such a way as to make the divergence vanish at time (i+1). This is reflected in Eq. (A-4) by setting only the $D_{j,k}^{i+1}$ term from expression (21) to zero, while the values at i and (i-1) are found from the velocity field at those times. In this way, any growth in the divergence field is self-limiting, and the solution remains stable.¹⁶

Equation (A-4) represents a Poisson equation for the pressure with the source term on the right a function of the latest iterate to the velocities at (i+1). It is solved here using a standard point SOR method, traversing the grid starting at the lower left corner (j = 2, k = 2), passing from left to right across each row, and sweeping from the bottom row up to the free surface. The initial condition is just the hydrostatic pressure distribution,

$$p_{j,k}^0 = p_{j,k+1}^0 + \left[\left(\frac{\xi_z}{\Delta \xi} \right)_{k+\frac{1}{2}} F \frac{H}{R} \right]^{-1}$$

the starting value for which is given by

$$p_{j,KT}^0 = p_{FS} + \left(\frac{\xi_{FS} - \xi_{KT}}{\Delta \xi} \right) \left[\left(\frac{\xi_z}{\Delta \xi} \right)_{KT-\frac{1}{2}} F \frac{H}{R} \right]^{-1}$$

The boundary conditions at the axis and solid boundaries are obtained by specializing the appropriate normal momentum difference equation to that boundary, and employing Eqs. (15) - (17). Hence at the centerline,

$$p_{1,k} = p_{2,k} \quad (22)$$

At the bottom wall,

$$\begin{aligned}
 p_{j,1} &= p_{j,2} + \left[\left(\frac{\xi_E}{\Delta \xi} \right)_{3/2} F \frac{H}{R} \right]^{-1} \\
 &+ 2 Re^{-1} r_j^{-1} \left(\frac{\rho_r}{\Delta \rho} \right)_j^{-1} \left[r_{j+\frac{1}{2}} u_{j+\frac{1}{2},2} - r_{j-\frac{1}{2}} u_{j-\frac{1}{2},2} \right]
 \end{aligned}
 \tag{23}$$

At the sidewall,

$$\begin{aligned}
 p_{NJ,k} &= p_{NJ-1,k} + \left(\frac{\rho_r}{\Delta \rho} \right)_{NJ-\frac{1}{2}}^{-1} \tilde{\Omega}^2 \\
 &+ 2 Re^{-1} \left(\frac{\xi_E}{\Delta \xi} \right)_k \left[\omega_{NJ-1,k+\frac{1}{2}} - \omega_{NJ-1,k-\frac{1}{2}} \right]
 \end{aligned}
 \tag{24}$$

where again $\tilde{\Omega}$ has been used rather than its final value of unity to allow for the ramped imposition of the sidewall boundary condition, cf. Eq. (18). The above represent Neumann-type boundary conditions on the solution; they are incorporated directly into the relaxation equations at the points immediately adjacent to the boundary as described by Roache¹⁹, pp. 183-184.

The pressure in the surface cell at (j, KT(j)) is found not from Eq. (A-4), but rather from the boundary condition that the pressure at the free surface be a constant, say p_{FS} . This boundary condition neglects the effects of surface tension, which are small for the surface radii of curvature of interest here.¹⁴ Also neglected are viscous stresses at the surface; their influence has been shown by experience to be significant only when $Re \lesssim 10$.²¹ Referring to Fig. 5, we denote by h the distance the free surface lies above the pressure node at KT, expressed in the transformed ξ coordinate. Then a linear interpolation between the surface and the node at KT-1 yields

$$p_{j,KT} = \left(p_{FS} + \frac{h}{\Delta \xi} p_{j,KT-1} \right) / \left(1 + \frac{h}{\Delta \xi} \right)
 \tag{25a}$$

21. Hirt, C.W. and Shannon, J.P., "Free-Surface Stress Conditions for Incompressible-Flow Calculations," J. of Computational Physics, Vol. 2, No. 4, 403-411, 1968.

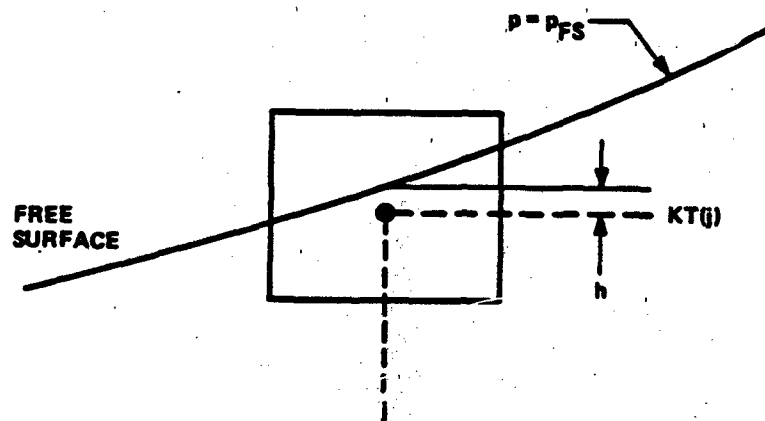


Figure 5 PRESSURE BOUNDARY CONDITION AT THE FREE SURFACE

Similarly, if the value at $KT+1$ should be needed,

$$p_{j,KT+1} = 2p_{j,KT} - p_{j,KT-1} \quad (25b)$$

Hence only in interior cells is the pressure adjusted to satisfy Eq. (20); in surface cells this function is served by the velocity boundary conditions, Eq. (19), with Eq. (25a) used to determine the pressure.

3.6 Difference Equation For Surface Contour

The continuous function $Z_{FS}(\rho, t)$ in Eq. (13) is discretized by defining it at integral values of j , i.e. Z_{FSj}^i denotes Z_{FS} at $\rho = \rho_j$ and $t = i \Delta t$. Second-order backward differences are again used for the time derivative. The convective term on the right is approximated using a hybrid of upwind and centered differences analogous to that used in the momentum equations.¹⁸ The result is

$$\frac{3Z_{FSj}^{n+1} - 4Z_{FSj}^n + Z_{FSj}^{n-1}}{2\Delta t} = w_{FSj}^{n+1} - \frac{1}{4} \left(\frac{\rho_r}{\Delta \rho} \right)_j \left[(u_{FSj-\frac{1}{2}}^{n+1} + u_{FSj+\frac{1}{2}}^{n+1}) (Z_{FSj+1}^{n+1} - Z_{FSj-1}^{n+1}) - \beta |u_{FSj-\frac{1}{2}}^{n+1} + u_{FSj+\frac{1}{2}}^{n+1}| (Z_{FSj+1}^{n+1} - 2Z_{FSj}^{n+1} + Z_{FSj-1}^{n+1}) \right] \quad (26)$$

where β is an input parameter analogous to α ; values of $\beta = 0$ and 1 produce purely centered and upwind differencing, respectively. Z_{FSj}^{n+1} represents the $(n+1)$ iterate to the contour Z_{FSj}^{i+1} , and w_{FSj}^{n+1} the free surface axial velocity at $\rho = \rho_j$, $z = Z_{FSj}^n$ found by linear interpolation of the $(n+1)$ velocity iterate. Eq. (26) represents a linear, tridiagonal system for the unknown Z_{FSj}^{n+1} , and so can be inverted using the same efficient algorithm as for the momentum equations. The initial condition is $Z_{FSj} = L/R$ at $t = 0$ for all j .

Since Eq. (13) is of first order in the radial coordinate, only a single boundary condition is required. But the values of Z_{FS} at the centerline and the sidewall are

not known a priori. So instead, a global boundary condition is employed, based on the fact that total fluid volume is conserved. At each instant this requires, in dimensionless form,

$$\sum_{j=2}^{NJ-1} r_j Z_{FSj} \left(\frac{d\rho}{dr} \right)_j^{-1} \Delta\rho = V_0 \quad (27)$$

The above summation is a trapezoidal rule approximation to the volume integral, in terms of the transformed variable ρ . The constant V_0 is easily determined at the start when all the Z_{FSj} equal the initial fill level. To see how this condition is enforced, we note that the last step in the tridiagonal solution algorithm¹⁹ for the Z^{n+1}_{FSj} is the application of the following linear recursion between neighboring values:

$$Z_{FSj}^{n+1} = E_j Z_{FSj+1}^{n+1} + F_j \quad (28)$$

E_j and F_j represent coefficients derived from Eq. (26) which depend on the surface velocities and β , but not on the Z^{n+1}_{FSj} :

From Eq. (28) we see that once the fluid level at $j = NJ$ is given any value the remainder of the contour is uniquely determined. So also is the summation in Eq. (27), which in general would not equal V_0 . However, since Eq. (28) is linear in Z_{FSj} one can easily substitute it into Eq. (27) and solve analytically for the value at $j = NJ$, in terms of V_0 and other constants, all of which are already known. In this way, the needed boundary condition on the surface contour is determined so as to automatically satisfy conservation of fluid volume without the need for additional iteration.

3.7 Overall Computational Cycle

Here we outline the principal steps involved in advancing the solution through one time cycle using the results of the preceding sections.

1. It is assumed that the solution at time levels i , $i-1$, and $i-2$ is known, either from the initial conditions, or because we have marched the calculation that far.

2. A prediction is made for each of the velocity components, the pressure, and the surface contour using the extrapolation in Eq. (14). This can be viewed as the zeroth iterate to the solution at $i+1$.
3. The velocity field is corrected, i.e. the $(n+1)$ st iterate is obtained from the solution of Eqs. (A-1) to (A-3), as described in Section 3.4.
4. The $(n+1)$ st iterate to the velocity field is used to interpolate for the radial and axial velocity components at the surface, and then Eq. (26) is solved for the $(n+1)$ st iterate to $Z^{i+1}FS_j$.
5. The boundary conditions on velocity and pressure across the new iterate to the free surface are updated using Eqs. (19) and (25).
6. Equation (A-4) is solved using point SOR to obtain the $(n+1)$ st iterate to the pressure field at time $(i+1)$. This actually represents an inner iteration nested inside the outer iteration loop for the velocity field. The pressure solution is considered to have converged when

$$\left(\frac{|\Delta p_{j,k}|}{\epsilon_{rp} |p_{j,k}^{n+1}| + \epsilon_{ap}} \right)_{\max_{j,k}} < 1 \quad (29)$$

where Δp_{jk} is the change in pressure at (j, k) from one pressure iteration to the next. ϵ_{rp} and ϵ_{ap} are, respectively, the relative and absolute convergence criteria applied to the pressure solution; typical values used are $\epsilon_{rp} = 10^{-4}$ and $\epsilon_{ap} = 10^{-6}$.

7. The pressure boundary condition across the free surface is updated using Eq. (25).

8. The convergence of the velocity field is assessed by testing whether

$$\left(\frac{|u_{j+\frac{1}{2},k}^{n+1} - u_{j+\frac{1}{2},k}^n|}{\epsilon_{rv} |u_{j+\frac{1}{2},k}^{n+1}| + \epsilon_{av}} \right)_{\text{MAX}_{j,k}} < 1 \quad (30)$$

with analogous tests applied to the v and w components as well. ϵ_{rv} and ϵ_{av} are the relative and absolute convergence criteria applied to the velocity field; typical values used are $\epsilon_{rv} = 10^{-3}$ and $\epsilon_{av} = 10^{-5}$. If Eq. (30) is not satisfied, return to Step 3 above for another iteration cycle.

9. Once Eq. (30) is satisfied, the $(n+1)$ st iterate is accepted as the new solution at $(i+1)$. The variable arrays are updated accordingly, and the divergence at the center of each cell is calculated and stored. If desired, printout of selected portions of the solution is made at this stage.
10. If a predetermined stop time or a steady-state condition has been reached, the calculation is halted. Otherwise, control returns to Step 2 for advancement through the next time cycle.

3.8 Results

The conditions chosen for initial study were $H/R = 3.0$, $Re = 10^3$, $F = 0.6$, $L/H = 0.8$, and $p\beta_5 = 0$. For these conditions the flow remains in Stage 1 (Figure 1) all the way to solid-body rotation, i.e., neither endwall is intersected. $NJ = 22$ and $NK = 32$ grid cells were used in the radial and axial directions, respectively, and the grid stretching parameters in Eqs. (9) and (10) were $b = c = 1.032$. These choices put the grid lines along $k = 2$ and $j = NJ-1$ at a distance 6.005×10^{-3} and 2.9×10^{-3} away from the endwall and sidewall, respectively. The parameters α and β were both zero, corresponding to centered differences.

Using various values of Δt , we unfortunately have not been able to run such a case to completion. Typically the calculation proceeds satisfactorily for a short time, but with a progressively slower convergence of the inner relaxation for the pressure field; the latter eventually fails to converge by the maximum allowed iteration cycle (ordinarily 40). Since the pressure field is determined in such a way as to enforce the continuity equation, diagnostics were added to the program to test whether Eq. (20) is

being accurately satisfied. These include evaluation of the largest absolute value of the divergence over the whole flow, where it occurred, and the root mean square value over all the grid cells. Also evaluated is the overall mass flux integral, which in dimensionless form can be approximated by

$$\begin{aligned} \dot{m} &= \int_{\mathcal{V}} (\nabla \cdot \vec{v}) d\mathcal{V} = 2\pi \int_{\mathcal{V}} (\nabla \cdot \vec{v}) r dr dz \\ &= 2\pi \int_{\mathcal{V}} (\nabla \cdot \vec{v}) r r_{\rho} z_{\xi} d\rho d\xi \\ &\approx 2\pi \sum_{j,k} D_{j,k} r_j \left(\frac{\rho_r}{\Delta\rho}\right)^{-1} \left(\frac{z_z}{\Delta z}\right)^{-1} \end{aligned}$$

Satisfaction of Eq. (20) thus assures local continuity while the magnitude of \dot{m} is a measure of global volume conservation.

With a relatively large time step of 0.5, when convergence breaks down the maximum absolute divergence and its r.m.s. value are approximately 8×10^{-2} and 6×10^{-3} , respectively, and \dot{m} is about -5×10^{-4} . These figures are unacceptably large; for comparison, the original MAC code (Ref. 16, p. 86) required that the maximum divergence should not exceed 3.5×10^{-3} . With a much smaller time step of 0.01, the maximum and r.m.s. values when convergence breaks down are 2×10^{-3} and 3×10^{-4} , respectively, with \dot{m} about 1×10^{-5} . While these values are more acceptable, the troublesome fact is that they appear to be steadily rising, rather than having levelled off. Evidently a source distribution is somehow being numerically introduced into the solution. Presumably the convergence criteria used in Eq. (29) will bear directly on the magnitude of $|D_{j,k}|$. But the criteria cited in Section 3.7 are if anything even more stringent than the $\epsilon_{rp} = 2 \times 10^{-4}$ of the MAC code (Ref. 16, p. 90).

The possibility of latent algebraic or FORTRAN errors is always present, but at this point must be viewed as remote. More likely is the possibility that the present semi-implicit method may be susceptible to instabilities not present in an explicit scheme (Roache¹⁹, p. 195). A review of the pertinent literature shows that Pracht²²

22. Pracht, W.E., "A Numerical Method for Calculating Transient Creep Flows," J. of Computational Physics, Vol. 7, 46-60, 1971.

and Aziz and Hellums²³ were the first to apply implicit methods to the full Navier-Stokes equations. Pracht's interest was primarily in low Reynolds number flows, $Re \leq 1$, for which the usual stability restriction on Δt for an explicit treatment of the viscous terms is prohibitively small. He was able to successfully calculate such flows with a larger Δt by treating just the diffusion and pressure gradient terms implicitly; convective terms were still evaluated at the previous time. Our interest here is primarily in higher Re , and an implicit treatment of all spatial derivatives. The first such attempt was that of Aziz and Hellums²³, who applied an Alternating-Direction-Implicit (ADI) scheme. They found that while this scheme worked well with a stream function-vorticity formulation of the equations, when cast in terms of primitive variables the equations required prohibitively small steps in order to satisfy continuity. They attributed this to the highly nonlinear coupling between the pressure and momentum equations.

Thus for confined flows the studies by Aziz and Hellums²³ and Kitchens¹⁵ indicate the stream function-vorticity formulation as the method of choice, since it allows satisfaction of the continuity equation ab initio. In the present problem the presence of the free surface does not easily admit such an approach, however. Further, hindsight suggests that the primitive variable approach taken in Ref. 23 may have been flawed in two respects. The first is that a conventional, as opposed to a staggered, grid was employed; as noted in Sections 3.3 and 3.5, this leads to an inconsistency between the momentum and pressure equations. More importantly, the $\partial D/\partial t$ term in the pressure equation needed to stabilize the growth of the divergence field was omitted.

More recently, Shadday, et al²⁴ have studied the steady flow in a rapidly rotating cylinder with a differentially rotating endcap as the asymptotic solution to the full transient equations. First order time differencing was used. To eliminate an otherwise severe restriction on Δt , they found it advantageous to treat the coriolis and pressure gradient terms implicitly. The remaining spatial derivatives were treated explicitly on a staggered grid, and the $\partial D/\partial t$ term was retained in the pressure equation.

-
23. Aziz, K. and Hellums, J.D., "Numerical Solution of the Three-Dimensional Equations of Motion for Laminar Natural Convection," *Physics of Fluids*, Vol. 10, No. 2, 314-324, 1967.
 24. Shadday, M.A., Ribando, R.J. and Kauzlarich, J.J., "Flow of an Incompressible Fluid in a Partially Filled, Rapidly Rotating Cylinder with a Differentially Rotating Endcap," *J. of Fluid Mechanics*, Vol. 130, 203-218, 1983.

The only successful attempts at using an implicit treatment for all spatial derivatives in the primitive variable equations appear to be those in Refs. 25-27. Hodge, et al.²⁵ employed first-order accurate backward differences for the time derivative. Spatial derivatives were all approximated to second order, with three-point "upwind" differences used for the convection terms. A point SOR method was used to iterate both the velocity and pressure equations at each time step. Hegna²⁶ later extended this scheme to incompressible turbulent flows. Despite the implicit nature of the algorithm, a time step $\Delta t < 0.001$ was found necessary to adequately follow the transient solution, resulting in CPU times of 2-4 hours (CDC Cyber 750).

Moitra²⁷ applied a similar scheme to the three-dimensional incompressible equations. He improved the time accuracy by employing second-order three-point backward time differencing in the momentum equations (as done here in Section 3.4); centered differences were used for all spatial derivatives, which were treated implicitly. Inexplicably however, only first-order accurate differencing was applied to the $\partial \rho / \partial t$ term in the Poisson equation for the pressure. This produces an inconsistency between the momentum and pressure equations, in addition to that introduced by his use of a conventional, rather than staggered, grid. Perhaps for these reasons, his solutions were found susceptible to "unusually high magnitudes of the divergence." To dampen this behavior, he introduces a spatially varying artificial viscosity proportional to the magnitude of the local divergence. To what degree this contaminates the numerical results remains an open question.

References 23-27 did not have a free surface, with the exception of Ref. 24; even then, Shadday, et al. assumed the free surface boundary conditions could be applied along a surface of constant radius, independent of time. Hence none of the above had the complication of a moving surface boundary condition to contend with. For example, this is what prevents us from using a more efficient direct-solver or spectral method

-
25. Hodge, J.K., Stone, A.L. and Miller, T.E., "Numerical Solution for Airfoils near Stall in Optimized Boundary-Fitted Curvilinear Coordinates," AIAA J., Vol. 17, No. 5, 458-464, May 1979.
 26. Hegna, H.A., "The Numerical Solution of Incompressible Turbulent Flow over Airfoils," AIAA Paper 81-0047, 19th Aerospace Sciences Meeting, 1981.
 27. Moitra, A., "An Implicit Solution of the Three-Dimensional Navier-Stokes Equations for an Airfoil Spanning a Wind Tunnel," Ph.D. Thesis, Dept. of Aerospace Engineering, Mississippi State University, 1982.

for inverting the Poisson equation for pressure; such methods are readily adaptable only to flows with relatively simple, stationary boundaries.

The present relaxation procedure for the pressure attempts to enforce the continuity equation by feeding back into the solution values of the divergence at time levels (i) and $(i - 1)$. Divergence values based on the new velocities at $(i + 1)$ do not appear because they are a priori assumed to be zero, in the spirit of the MAC method (cf. Section 3.5). Alternative methods have been proposed which use information about the divergence at time $(i + 1)$. For example, Hirt et al.¹⁸ compute the divergence in each cell based on the latest velocities. Then the pressure at the cell center is changed by an amount proportional to minus the divergence. Hence a positive (negative) value of D will produce a negative (positive) increment in p which acts to drive D toward zero. This recipe is followed from cell to cell in the flow; a constant of proportionality greater than one is often introduced to overrelax the solution. Such a procedure can be shown to be analogous to solving a Poisson equation for the pressure. It has the dual advantages over Eq. (A-4) of having a much simpler right hand side, and its direct use of the current divergence, as opposed to that at previous times. Whether it could successfully be incorporated with the present line relaxation for the velocity field will require further analysis.

To summarize, we have not yet been successful in our application of the PCMI algorithm to spin-up in a partially-filled cylinder. Our review of the pertinent literature has turned up several examples of the successful application of other implicit methods to the incompressible Navier-Stokes equations.²⁴⁻²⁷ The differencing scheme of Moitra²⁷ most closely parallels that used here, although significant differences remain in the grids used and the methods employed to solve the algebraic equations. Interestingly, his results also tended to exhibit unacceptably large values for the divergence of the velocity field. We are still in hopes that this instability can be removed without resorting to the explicit introduction of artificial viscosity used by Moitra, as the latter may unduly contaminate the results.

In any event, we have found no a priori reason to doubt the validity of the present approach. Nevertheless, the connected difficulties of slow convergence of the pressure iterations and the inaccurate satisfaction of the continuity equation need to be addressed. In the future we hope to study whether a pressure correction scheme based on the latest divergence iterates could successfully overcome these problems.

4. CONCLUSIONS

Initially a simplified numerical model was developed for the axisymmetric spin-up of fluid in a partially-filled cylindrical cavity. The analysis represents an extension of the earlier treatments by Wedemeyer,¹² and Goller and Ranov,¹¹ to those cases where the liquid free surface may intersect one or both endwalls. Earlier estimates of the Ekman layer pumping of the secondary flow are modified heuristically for situations where the layer no longer covers the entire wall. Also, due to the very steep free surface contour in the latter stages of spin-up, it was found advantageous to develop the free surface equations in an axial, rather than radial, coordinate frame.

A computer program was used to solve the governing nonlinear equations using a straightforward finite-difference algorithm. The code predicts both the azimuthal velocity distribution with radius, and the free surface contour, as functions of time. The results exhibit good agreement with the time-resolved experimental data for the surface contour taken by Goller and Ranov. Their data were taken only for situations where the free surface did not touch the endwalls. At present, there are no quantitative data against which the simplified analysis can be compared for cases where one or both endwalls are intersected.

Nevertheless, the following qualitative conclusions have been drawn from the theory. Plotting the fluid angular momentum deficit vs. $Re^{-1/2} t$ appears to correlate the numerical data reasonably well. Such plots indicate that the angular momentum transfer follows a simple exponential behavior in time. For Re in the range $10^3 - 10^5$, the growth rate appears uniform up to the point where the bottom endwall is intersected. After this, exponential behavior is still exhibited, but at a reduced rate, reflecting the diminishing influence of the bottom Ekman layer which is primarily responsible for the secondary flow. The magnitude of the reduction in spin-up rate diminishes with decreasing Reynolds number.

To validate the simplified model in a quantitative sense, it is desirable that its predictions be compared with suitably designed laboratory experiments and/or more refined numerical calculations. As an attempt to generate the latter, the second phase of this program was devoted to developing a numerical model based on the full, axisymmetric Navier-Stokes equations. In an effort to avoid the severe time step

restrictions characteristic of explicit algorithms, the semi-implicit Predictor-Corrector Multiple-Iteration (PCMI) finite difference scheme was applied to the equations in primitive variable form. Unfortunately, we have thus far only been able to march the calculation for a short time before its convergence breaks down. This seems to be related to an unacceptably large growth in the divergence of the velocity field, which should vanish.

Our review of the relevant literature has turned up several examples of the successful application of other implicit methods to the incompressible Navier-Stokes equations.²⁴⁻²⁷ But each differs in sufficient detail from the present scheme so as not to offer much guidance on how to resolve the difficulties. One complication we face which has not been previously addressed by other implicit methods is the presence of a moving free surface. In any event, we have found no a priori reason to doubt the ultimate applicability of the PCMI method to this problem. Nevertheless, the connected difficulties of slow convergence of the pressure iterations and the inaccurate satisfaction of the continuity equation need to be addressed. In the future we hope to study whether a pressure correction scheme based on the latest divergence iterates could successfully overcome these problems.

REFERENCES

1. Engineering Design Handbook. Liquid-Filled Projectile Design, AMC Pamphlet No. 706-165, U.S. Army Materiel Command, Washington, D.C., April 1969.
2. Kitchens, C.W., Jr., Gerber, N. and Sedney, R., "Spin Decay of Liquid-Filled Projectiles," J. of Spacecraft, Vol. 15, No. 6, 348-354, December 1978.
3. Kitchens, C.W., Jr. and Gerber, N., Prediction of Spin Decay of Liquid-Filled Projectiles, BRL Report 1996, Aberdeen Proving Ground, Md., July 1977.
4. Kitchens, C.W., Jr., Gerber, N., and Sedney, R., Oscillations of a Liquid in a Rotating Cylinder: Part I. Solid-Body Rotation, ARBRL-TR-02081, Aberdeen Proving Ground, Md., June 1978.
5. Sedney, R., and Gerber, N., Oscillations of a Liquid in a Rotating Cylinder: Part II. Spin-Up, ARBRL-TR-02489, Aberdeen Proving Ground, Md., May 1983.
6. Homicz, G. F., Numerical Model for Fluid Spin-Up in a Partially-Filled Cylinder, Calspan Report No. 6856-A-1, May 1982, prepared for U.S. Army Research Office as interim report on Contract DAAG29-81-C-0007.
7. Homicz, G. F. and Gerber, N., "Numerical Model for Fluid Spin-Up from Rest in a Partially-Filled Cylinder," submitted to ASME Transactions, J. of Fluids Engineering.
8. Greenspan, H.P., The Theory of Rotating Fluids, Cambridge University Press, London, 1968.
9. Mark, A., Measurements of Angular Momentum Transfer in Liquid-Filled Projectiles, ARBRL-TR-2029, Aberdeen Proving Ground, Md., November 1977.
10. Gerber, N., "Properties of Rigidly Rotating Liquids in Closed Partially Filled Cylinders," ASME Transactions, J. of Applied Mechanics, Vol. 97, 734-735, 1975.
11. Goller, H. and Ranov, T., "Unsteady Rotating Flow in a Cylinder with a Free Surface," ASME Transactions, J. of Basic Engineering, Vol. 90D, No. 4, 445-454, December 1968.
12. Wedemeyer, E.H., "The Unsteady Flow Within a Spinning Cylinder," J. of Fluid Mechanics, Vol. 20 Pt. 3, 383-399, 1964.
13. Pismen, L.M. and Nir, A., "Motion of a Contact Line," Physics of Fluids, Vol. 25, No. 1, 3-7, January 1982.
14. Batchelor, G. K., An Introduction to Fluid Dynamics, Cambridge University Press, 1967.
15. Kitchens, C.W., Jr., "Navier-Stokes Solutions for Spin-Up in a Filled Cylinder," AIAA J., Vol. 18, No. 8, 929-934, August 1980.

16. Welch, J.E., Harlow, F. E., Shannon, J.P. and Daly, B.J., The MAC Method: A Computing Technique for Solving Viscous, Incompressible, Transient Fluid-Flow Problems Involving Free Surfaces, Los Alamos Scientific Laboratory Report LA-3425, March 1966.
17. Rubin, S. G. and Lin, T. C., "A Numerical Method for Three-Dimensional Viscous Flow: Application to the Hypersonic Leading Edge," J. of Computational Physics, Vol. 9, 339-364, 1972.
18. Hirt, C. W., Nichols, B. D., and Romero, N. C., SOLA - A Numerical Solution Algorithm for Transient Fluid Flows, Los Alamos Scientific Laboratory Report LA-5852, April 1975.
19. Roache, P. J., Computational Fluid Dynamics, Hermosa Publishers, Albuquerque, N.M., 1976.
20. Spalding, D. B., "A Novel Finite Difference Formulation for Differential Expressions Involving both First and Second Derivatives," International Journal for Numerical Methods in Engineering, Vol. 4, 551-559, 1972.
21. Hirt, C.W. and Shannon, J.P., "Free-Surface Stress Conditions for Incompressible-Flow Calculations," J. of Computational Physics, Vol. 2, No. 4, 403-411, 1968.
22. Pracht, W.E., "A Numerical Method for Calculating Transient Creep Flows," J. of Computational Physics, Vol. 7, 46-60, 1971.
23. Aziz, K. and Hellums, J.D., "Numerical Solution of the Three-Dimensional Equations of Motion for Laminar Natural Convection," Physics of Fluids, Vol. 10, No. 2, 314-324, 1967.
24. Shadday, M.A., Ribando, R.J. and Kauzlarich, J.J., "Flow of an Incompressible Fluid in a Partially Filled, Rapidly Rotating Cylinder with a Differentially Rotating Endcap," J. of Fluid Mechanics, Vol. 130, 203-218, 1983.
25. Hodge, J.K., Stone, A.L. and Miller, T.E., "Numerical Solution for Airfoils near Stall in Optimized Boundary-Fitted Curvilinear Coordinates," AIAA J., Vol. 17, No. 5, 458-464, May 1979.
26. Hegna, H.A., The Numerical Solution of Incompressible Turbulent Flow over Airfoils, AIAA Paper 81-0047, 19th Aerospace Sciences Meeting, 1981.
27. Moitra, A., An Implicit Solution of the Three-Dimensional Navier-Stokes Equations for an Airfoil Spanning a Wind Tunnel, Ph.D. Thesis, Dept. of Aerospace Engineering, Mississippi State University, 1982.

NOMENCLATURE

b,c	grid stretching parameters in Eqs. (9) and (10)
D	divergence of the velocity field
F	Froude number, $(\Omega R)^2/gH$
g	axial acceleration (= gravity in a laboratory frame)
H	height of cylinder
i	time index
j	radial grid index
k	axial grid index
L	initial fluid level before spin-up
L_z	dimensionless fluid angular momentum about the cylinder's axis
NJ, NK	number of radial, axial grid cells, respectively
p	dimensionless pressure, $p/\rho (\Omega R)^2$
PFS	dimensionless free surface pressure
$\bar{r}, \bar{\theta}, \bar{z}$	dimensional cylindrical coordinates
R	radius of cylinder
r	r/R
r_0, r_H	dimensionless radii at which endwalls are intersected (Figure 1)
RFS	radial coordinate description of the free surface during Stage 3
Re	Reynolds number, $\Omega R^2/\nu$
t	$\Omega \bar{t}$
t_s	dimensionless spin-up, time
u,v,w	dimensionless velocities in the (r, θ , z) directions, respectively, normalized by ΩR
z	\bar{z}/H in simplified model; \bar{z}/R in Navier-Stokes code.
ZFS	axial coordinate description of the free surface during Stages 1 and 2b
α, β	parameters used to adjust degree of upwind differencing, Eqs. (26), (A-1)-(A-3)
ϵ_r, ϵ_a	relative and absolute error criteria used in Eqs. (29) and (30).
ν	kinematic viscosity
ρ	density
ξ, ρ	axial, radial coordinates in the computational plane
Ω	final angular velocity of cylinder, rad./sec.
$\bar{\Omega}$	dimensionless angular velocity of cylinder, normalized by Ω
ω	dimensionless local fluid angular velocity, $v/r = \bar{\omega}/\Omega$
()	indicates a dimensional variable

APPENDIX

We quote here the full difference equations for the velocity components and pressure, which are somewhat lengthy to include in the main text. The differencing procedure for the u, v, and w equations is described in Section 3.4, and the results are:

u equation

$$\begin{aligned}
 & \frac{3u_{j+\frac{1}{2}k}^{n+1} - 4u_{j+\frac{1}{2}k}^n + u_{j+\frac{1}{2}k}^{n-1}}{2\Delta t} \\
 & + \frac{1}{4r_{j+\frac{1}{2}}} \left(\frac{\rho_r}{\Delta\rho} \right)_{j+\frac{1}{2}} \left\{ r_{j+1} \left[(u_{j+\frac{1}{2},k}^n + u_{j+\frac{3}{2},k}^n) (u_{j+\frac{1}{2},k}^{n+1} + u_{j+\frac{3}{2},k}^{n+1}) \right. \right. \\
 & \quad \left. \left. + \alpha |u_{j+\frac{1}{2},k}^n + u_{j+\frac{3}{2},k}^n| (u_{j+\frac{1}{2},k}^{n+1} - u_{j+\frac{3}{2},k}^{n+1}) \right] \right. \\
 & \quad \left. - r_j \left[(u_{j-\frac{1}{2},k}^n + u_{j+\frac{1}{2},k}^n) (u_{j-\frac{1}{2},k}^{n+1} + u_{j+\frac{1}{2},k}^{n+1}) \right. \right. \\
 & \quad \left. \left. + \alpha |u_{j-\frac{1}{2},k}^n + u_{j+\frac{1}{2},k}^n| (u_{j-\frac{1}{2},k}^{n+1} - u_{j+\frac{1}{2},k}^{n+1}) \right] \right\} - r_{j+\frac{1}{2}}^{-1} (v_{j+\frac{1}{2}k}^n)^2 \\
 & + \frac{1}{4} \left(\frac{S_z}{\Delta\xi} \right)_k \left\{ (\omega_{jk+\frac{1}{2}}^n + \omega_{j+1,k+\frac{1}{2}}^n) (u_{j+\frac{1}{2}k}^{n+1} + u_{j+\frac{1}{2}k+1}^n) \right. \\
 & \quad \left. + \alpha |\omega_{jk+\frac{1}{2}}^n + \omega_{j+1,k+\frac{1}{2}}^n| (u_{j+\frac{1}{2}k}^{n+1} - u_{j+\frac{1}{2}k+1}^n) \right. \\
 & \quad \left. - (\omega_{jk-\frac{1}{2}}^{n+1} + \omega_{j+1,k-\frac{1}{2}}^{n+1}) (u_{j+\frac{1}{2}k-1}^{n+1} + u_{j+\frac{1}{2}k}^{n+1}) \right. \\
 & \quad \left. - \alpha |\omega_{jk-\frac{1}{2}}^{n+1} + \omega_{j+1,k-\frac{1}{2}}^{n+1}| (u_{j+\frac{1}{2}k-1}^{n+1} - u_{j+\frac{1}{2}k}^{n+1}) \right\} \\
 & - \left(\frac{\rho_r}{\Delta\rho} \right)_{j+\frac{1}{2}} (p_{j+1k}^n - p_{jk}^n)
 \end{aligned}$$

$$\begin{aligned}
 - R_c^{-1} \left(\frac{\xi_z}{\Delta \xi} \right)_k \left\{ \left(\frac{\xi_z}{\Delta \xi} \right)_{k+\frac{1}{2}} (u_{j+\frac{1}{2},k+1}^n - u_{j+\frac{1}{2},k}^{n+1}) - \left(\frac{\rho_r}{\Delta \rho} \right)_{j+\frac{1}{2}} (\omega_{j+1,k+\frac{1}{2}}^n - \omega_{j,k+\frac{1}{2}}^n) \right. \\
 \left. - \left(\frac{\xi_z}{\Delta \xi} \right)_{k-\frac{1}{2}} (u_{j+\frac{1}{2},k}^{n+1} - u_{j+\frac{1}{2},k-1}^{n+1}) + \left(\frac{\rho_r}{\Delta \rho} \right)_{j+\frac{1}{2}} (\omega_{j+1,k-\frac{1}{2}}^{n+1} - \omega_{j,k-\frac{1}{2}}^{n+1}) \right\} = 0 \quad (A-1)
 \end{aligned}$$

In writing Eq. (A-1), updated values have been used as soon as they become available. Since the grid is swept from bottom to top, this means using the (n+1) iterate for velocities in cells centered on row k and below; above this line, values from the (n)th iterate are used. This scheme also saves considerable storage, since the (n+1) and (n)th iterates need not be stored simultaneously; i.e., a single array is used with the former replacing the latter as soon as it is calculated.

v equation

$$\begin{aligned}
 \frac{3v_{j+\frac{1}{2},k}^{n+1} - 4v_{j+\frac{1}{2},k}^i + v_{j+\frac{1}{2},k}^{i-1}}{2\Delta t} \\
 + \frac{1}{4r_{j+\frac{1}{2}}} \left(\frac{\rho_r}{\Delta \rho} \right)_{j+\frac{1}{2}} \left\{ r_{j+1} [(u_{j+\frac{1}{2},k}^n + u_{j+\frac{3}{2},k}^n) (v_{j+\frac{1}{2},k}^{n+1} + v_{j+\frac{3}{2},k}^{n+1}) \right. \\
 + \alpha |u_{j+\frac{1}{2},k}^n + u_{j+\frac{3}{2},k}^n| (v_{j+\frac{1}{2},k}^{n+1} - v_{j+\frac{3}{2},k}^{n+1})] \\
 - r_j [(u_{j-\frac{1}{2},k}^n + u_{j+\frac{1}{2},k}^n) (v_{j-\frac{1}{2},k}^{n+1} + v_{j+\frac{1}{2},k}^{n+1}) \\
 \left. + \alpha |u_{j-\frac{1}{2},k}^n + u_{j+\frac{1}{2},k}^n| (v_{j-\frac{1}{2},k}^{n+1} - v_{j+\frac{1}{2},k}^{n+1})] \right\} + r_{j+\frac{1}{2}}^{-1} u_{j+\frac{1}{2},k}^n v_{j+\frac{1}{2},k}^{n+1} \\
 + \frac{1}{4} \left(\frac{\xi_z}{\Delta \xi} \right)_k \left\{ (\omega_{j,k+\frac{1}{2}}^n + \omega_{j+1,k+\frac{1}{2}}^n) (v_{j+\frac{1}{2},k}^{n+1} + v_{j+\frac{1}{2},k+1}^n) \right. \\
 + \alpha |\omega_{j,k+\frac{1}{2}}^n + \omega_{j+1,k+\frac{1}{2}}^n| (v_{j+\frac{1}{2},k}^{n+1} - v_{j+\frac{1}{2},k+1}^n) \\
 - (\omega_{j,k-\frac{1}{2}}^{n+1} + \omega_{j+1,k-\frac{1}{2}}^{n+1}) (v_{j+\frac{1}{2},k-1}^{n+1} + v_{j+\frac{1}{2},k}^{n+1}) \\
 \left. - \alpha |\omega_{j,k-\frac{1}{2}}^{n+1} + \omega_{j+1,k-\frac{1}{2}}^{n+1}| (v_{j+\frac{1}{2},k-1}^{n+1} - v_{j+\frac{1}{2},k}^{n+1}) \right\}
 \end{aligned}$$

$$\begin{aligned}
& - R e^{-1} \left\{ \left(\frac{\rho_r}{\Delta \rho} \right)_{j+\frac{1}{2}} \left[r_{j+\frac{1}{2}}^{-1} \left(\frac{\rho_r}{\Delta \rho} \right)_{j+\frac{1}{2}} \left(r_{j+\frac{3}{2}} v_{j+\frac{3}{2},k}^{n+1} - r_{j+\frac{1}{2}} v_{j+\frac{1}{2},k}^{n+1} \right) \right. \right. \\
& \quad \left. \left. - r_j^{-1} \left(\frac{\rho_r}{\Delta \rho} \right)_j \left(r_{j+\frac{1}{2}} v_{j+\frac{1}{2},k}^{n+1} - r_{j-\frac{1}{2}} v_{j-\frac{1}{2},k}^{n+1} \right) \right] \right. \\
& \quad \left. + \left(\frac{\xi_z}{\Delta \xi} \right)_k \left[\left(\frac{\xi_z}{\Delta \xi} \right)_{k+\frac{1}{2}} \left(v_{j+\frac{1}{2},k+1}^n - v_{j+\frac{1}{2},k}^n \right) \right. \right. \\
& \quad \left. \left. - \left(\frac{\xi_z}{\Delta \xi} \right)_{k-\frac{1}{2}} \left[\left(v_{j+\frac{1}{2},k}^{n+1} - v_{j+\frac{1}{2},k-1}^{n+1} \right) \right] \right] \right\} = 0 \quad (A-2)
\end{aligned}$$

w equation

$$\begin{aligned}
& \frac{3\omega_{j,k+\frac{1}{2}}^{n+1} - 4\omega_{j,k+\frac{1}{2}}^n + \omega_{j,k+\frac{1}{2}}^{n-1}}{2\Delta t} \\
& + \frac{1}{4r_j} \left(\frac{\rho_r}{\Delta \rho} \right)_j \left\{ r_{j+\frac{1}{2}} \left[\left(u_{j+\frac{1}{2},k}^n + u_{j+\frac{1}{2},k+1}^n \right) \left(\omega_{j,k+\frac{1}{2}}^{n+1} + \omega_{j,k+\frac{1}{2}}^n \right) \right. \right. \\
& \quad \left. \left. + \alpha \left| u_{j+\frac{1}{2},k}^n + u_{j+\frac{1}{2},k+1}^n \right| \left(\omega_{j,k+\frac{1}{2}}^{n+1} - \omega_{j+1,k+\frac{1}{2}}^{n+1} \right) \right] \right. \\
& \quad \left. - r_{j-\frac{1}{2}} \left[\left(u_{j-\frac{1}{2},k}^n + u_{j-\frac{1}{2},k+1}^n \right) \left(\omega_{j-1,k+\frac{1}{2}}^{n+1} + \omega_{j,k+\frac{1}{2}}^n \right) \right. \right. \\
& \quad \left. \left. + \alpha \left| u_{j-\frac{1}{2},k}^n + u_{j-\frac{1}{2},k+1}^n \right| \left(\omega_{j-1,k+\frac{1}{2}}^{n+1} - \omega_{j,k+\frac{1}{2}}^n \right) \right] \right\} \\
& + \frac{1}{4} \left(\frac{\xi_z}{\Delta \xi} \right)_{k+\frac{1}{2}} \left\{ \left(\omega_{j,k+\frac{1}{2}}^n + \omega_{j,k+\frac{3}{2}}^n \right) \left(\omega_{j,k+\frac{1}{2}}^{n+1} + \omega_{j,k+\frac{3}{2}}^n \right) \right. \\
& \quad \left. + \alpha \left| \omega_{j,k+\frac{1}{2}}^n + \omega_{j,k+\frac{3}{2}}^n \right| \left(\omega_{j,k+\frac{3}{2}}^{n+1} - \omega_{j,k+\frac{1}{2}}^n \right) \right\}
\end{aligned}$$

$$\begin{aligned}
& - (\omega_{jk-\frac{1}{2}}^{n+1} + \omega_{jk+\frac{1}{2}}^n) (\omega_{jk-\frac{1}{2}}^{n+1} + \omega_{jk+\frac{1}{2}}^{n+1}) \\
& - \alpha \left| \omega_{jk-\frac{1}{2}}^{n+1} + \omega_{jk+\frac{1}{2}}^n \right| (\omega_{jk-\frac{1}{2}}^{n+1} - \omega_{jk+\frac{1}{2}}^{n+1}) \Big\} \\
& + \left(\frac{\xi_x}{\Delta \xi} \right)_{k+\frac{1}{2}} (p_{jk+1}^n - p_{jk}^n) + \left(F \frac{H}{R} \right)^{-1}
\end{aligned}$$

(A-3)

$$\begin{aligned}
- R e^{-1} r_j^{-1} \left(\frac{\rho_r}{\Delta \rho} \right)_j \left\{ r_{j+\frac{1}{2}} \left[\left(\frac{\rho_r}{\Delta \rho} \right)_{j+\frac{1}{2}} (\omega_{j+1, k+\frac{1}{2}}^{n+1} - \omega_{jk+\frac{1}{2}}^{n+1}) - \left(\frac{\xi_x}{\Delta \xi} \right)_{k+\frac{1}{2}} (u_{j+\frac{1}{2}, k+1}^n - u_{j+\frac{1}{2}, k}^n) \right] \right. \\
\left. - r_{j-\frac{1}{2}} \left(\frac{\rho_r}{\Delta \rho} \right)_{j-\frac{1}{2}} (\omega_{jk+\frac{1}{2}}^{n+1} - \omega_{j-1, k+\frac{1}{2}}^{n+1}) - \left(\frac{\xi_x}{\Delta \xi} \right)_{k+\frac{1}{2}} (u_{j-\frac{1}{2}, k+1}^n - u_{j-\frac{1}{2}, k}^n) \right\} = 0
\end{aligned}$$

The above equations are tridiagonal in the (n+1) iterate values on each row k.

The difference equation for the pressure is obtained from a linear combination of Eq. (A-1) and (A-3), as described in Section 3.5. The full result is, for $\alpha = 0$,

$$\begin{aligned}
& r_j^{-1} \left(\frac{\rho_r}{\Delta \rho} \right)_j \left[r_{j+\frac{1}{2}} \left(\frac{\rho_r}{\Delta \rho} \right)_{j+\frac{1}{2}} (p_{j+1, k}^{n+1} - p_{j, k}^{n+1}) - r_{j-\frac{1}{2}} \left(\frac{\rho_r}{\Delta \rho} \right)_{j-\frac{1}{2}} (p_{j, k}^{n+1} - p_{j-1, k}^{n+1}) \right] \\
& + \left(\frac{\xi_x}{\Delta \xi} \right)_k \left[\left(\frac{\xi_x}{\Delta \xi} \right)_{k+\frac{1}{2}} (p_{j, k+1}^{n+1} - p_{j, k}^{n+1}) - \left(\frac{\xi_x}{\Delta \xi} \right)_{k-\frac{1}{2}} (p_{j, k}^{n+1} - p_{j, k-1}^{n+1}) \right] \\
& = \frac{4D_{j, k}^i - D_{j, k}^{i-1}}{2\Delta t} - \left[\left(\frac{\rho_r}{\Delta \rho} \right)_j (u_{j+\frac{1}{2}, k}^{n+1} - u_{j-\frac{1}{2}, k}^{n+1}) \right]^2 - \left[\frac{u_{j+\frac{1}{2}, k}^{n+1} + u_{j-\frac{1}{2}, k}^{n+1}}{2r_j} \right]^2 \\
& + \frac{1}{r_j} \left(\frac{\rho_r}{\Delta \rho} \right)_j \left[(v_{j+\frac{1}{2}, k}^{n+1})^2 - (v_{j-\frac{1}{2}, k}^{n+1})^2 \right] - \left[\left(\frac{\xi_x}{\Delta \xi} \right)_k (\omega_{j, k+\frac{1}{2}}^{n+1} - \omega_{j, k-\frac{1}{2}}^{n+1}) \right]^2 \\
& - \frac{1}{\theta} \left(\frac{\xi_x}{\Delta \xi} \right)_k \left(\frac{\rho_r}{\Delta \rho} \right)_j (u_{j-\frac{1}{2}, k+1}^{n+1} + u_{j+\frac{1}{2}, k+1}^{n+1} - u_{j-\frac{1}{2}, k-1}^{n+1} - u_{j+\frac{1}{2}, k-1}^{n+1}) \\
& \quad \times (\omega_{j+1, k+\frac{1}{2}}^{n+1} + \omega_{j+1, k-\frac{1}{2}}^{n+1} - \omega_{j-1, k+\frac{1}{2}}^{n+1} - \omega_{j-1, k-\frac{1}{2}}^{n+1})
\end{aligned} \tag{A-4}$$

Terms involving D^{i+1} have already been set to zero to satisfy the incompressibility condition at the new time, while recognizing that D^i and D^{i-1} will in general carry small residual values.

TECHNICAL REPORTS, PUBLICATIONS

Homicz, G.F., Numerical Model for Fluid Spin-Up in a Partially-Filled Cylinder, Calspan Report No. 6856-A-1, May 1982, prepared for U.S. Army Research Office as interim report on Contract DAAG29-81-C-0007.

Homicz, G.F., "Numerical Model for Fluid Spin-Up in a Partially-Filled Cylinder," presented at ARRADCOM Conference on Aeroballistics and Fluid Dynamics Technology for the 80's, Downingtown, Pa., Sept. 28-30, 1982.

Homicz, G.F. and Gerber, N., "Numerical Model for Fluid Spin-Up from Rest in a Partially-Filled Cylinder," submitted to ASME Transactions, J. of Fluids Engineering.